BCSJ

Document type: Review/Account

Account/Review for Frontiers of Molecular Science
Account/Review for Life Chemistry
Award Account

The Chemical Society of Japan Award for Young Chemists for 2017

Syntheses and Characterizations of Functional Polycyclic Aromatic Hydrocarbons and Graphene Nanoribbons

Xiushang Xu,[1,2] Klaus Müllen,*[1,3] and Akimitsu Narita*[1,2]

[1]Max Planck Institute for Polymer Research, Ackermannweg 10, 55128, Mainz, Germany

[2]Organic and Carbon Nanomaterials Unit, Okinawa Institute of Science and Technology Graduate University, 1919-1 Tancha, Onna-son, Kunigami, Okinawa 904-0495, Japan

[3]Institute of Physical Chemistry, Johannes Gutenberg-Universität Mainz, Duesbergweg 10-14, 55128 Mainz, Germany

E-mail: narita@mpip-mainz.mpg.de (A. Narita), muellen@mpip-mainz.mpg.de (K. Müllen)

Received: December 23, 2019; Accepted: January 17, 2020; Web Released: January 24, 2020

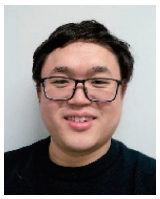

Xiushang Xu
Xiushang Xu received his PhD at the Changchun Institute of Applied Chemistry, Chinese Academy of Sciences under supervision of Professor Lixiang Wang in January, 2019. Since April 2019, he has been a postdoctoral researcher in the Narita Unit at the Okinawa Institute of Science and Technology Graduate University (OIST), and also a guest scientist at the Max Planck Institute for Polymer Research (MPIP) in Mainz, Germany. His current research interest focuses on the bottom-up synthesis of novel nanocarbon materials with atomically precise structures for the elucidation of their optical and electronic properties and applications for optoelectronic devices and bioimaging.

Klaus Müllen
Klaus Müllen studied chemistry at the University of Cologne and received his PhD from the University of Basel in 1971. After postdoctoral research and his habilitation at ETH Zurich, he joined the University of Cologne as a Professor in 1979 and moved to the University of Mainz in 1984. From 1989 to 2016 he was Director of the Synthetic Chemistry Department at MPIP. Since 2016 he has been an emeritus director and the leader of an emeritus group at MPIP as well as a Gutenberg Research Fellow at the Johannes Gutenberg University of Mainz (JGU). His current research focuses on synthetic macromolecular chemistry, supramolecular chemistry, and materials science.

Akimitsu Narita 【Award recipient】
Akimitsu Narita studied chemistry at the University of Tokyo, where he received his Bachelor's (2008) and Master's (2010) degrees under the supervision of Professor Eiichi Nakamura. He then joined the group of Professor Klaus Müllen at MPIP, and obtained his PhD in Chemistry in 2014, granted by JGU. Since 2014 he has been a Project Leader in the Synthetic Chemistry Department at MPIP. In 2018 he joined OIST as an Assistant Professor (Adjunct) leading the Organic and Carbon Nanomaterials Unit. His current research focuses on the bottom-up synthesis of functional nanocarbon materials, especially nanographenes and graphene nanoribbons, with atomically precise chemical structures. He received the Chemical Society of Japan Award for Young Chemists for 2017.

Abstract

In contrast to zero-bandgap graphene, nanostructures of graphene, such as graphene quantum dots (GQDs) and graphene nanoribbons (GNRs) have open bandgaps due to the quantum confinement effect, and are thus highly interesting for semiconductor applications, for example in nanoelectronics and

optoelectronics. While conventional methods cannot provide GQDs and GNRs with chemically precise structures, large polycyclic aromatic hydrocarbon (PAH) molecules can be regarded as atomically precise GQDs. Moreover, extension of the PAH synthesis can lead to GNRs with well-defined chemical structures. In this account, we summarize our recent achievements in our synthetic exploration of PAHs and GNRs with novel structures and properties. For example, we have developed new PAHs having zigzag edges, such as dibenzo[*hi*,*st*]ovalene derivatives with strong red luminescence and stimulated emission, which are promising for light-emitting devices and bioimaging applications. We have also accomplished a synthesis of magnetic GNRs through edge functionalization with organic radicals, which can be interesting for spintronic as well as quantum computing applications. Moreover, incorporation of zigzag edges in GNR structures, through on-surface syntheses under ultrahigh (UHV) vacuum conditions, allowed for significant modulations of the electronic structures of GNRs, leading to the emergence of topological quantum phases. On the other hand, we have also explored on-surface synthesis of GNRs without UHV, namely using a setup for chemical vapor deposition (CVD). Scalable fabrication of GNR films could thus be achieved on gold on mica substrates, which could be integrated into field-effect transistor devices. These results highlight the importance of developing novel PAHs and GNRs and their potentials for various applications, including quantum technologies, energy and optoelectronic devices, and bioimaging.

Keywords: Polycyclic aromatic hydrocarbon | Nanographene | Graphene nanoribbon

1. Introduction

Graphene, namely monolayer graphite, has been widely investigated as a fascinating material since its first experimental demonstration by Geim and Novoselov in 2004.[1] In particular, excellent charge-carrier mobilities of graphene attracted numerous research groups and companies worldwide to explore graphene-based electronic devices for future applications,[2–5] ranging from nanoelectronics[6] and flexible electronics[7] to biosensing[8,9] and disease diagnostics.[10] Nevertheless, graphene is a zero-bandgap material, which prohibits its use as an active semiconductor material, since the electric conduction cannot be switched off without a bandgap.[11–15] In contrast, nanostructures of graphene, such as graphene quantum dots (GQDs) and graphene nanoribbons (GNRs), possess open bandgaps when they are small enough to experience the quantum confinement effect, and are thus highly promising for semiconductor applications.[12,16–20]

Early theoretical studies have already revealed that the electronic properties, including the bandgaps, of GQDs and GNRs are dependent on their edge structure and size or width.[21–26] For example, GNRs with zigzag edges (zigzag GNRs, or ZGNRs, e.g., 6-ZGNR in Figure 1a and c) were predicted to have edge-localized states that can be spin-polarized together with a zero bandgap at the tight-binding level of theory.[23,27] In contrast, GNRs with armchair edges (armchair GNRs, or AGNRs, e.g., 9-AGNR in Figure 1b and d) were calculated to have larger

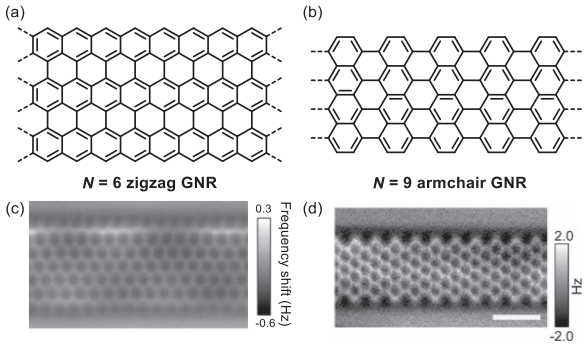

Figure 1. Structures of (a) $N = 6$ zigzag GNR (6-ZGNR) and (b) $N = 9$ armchair GNR (9-AGNR). (c) Constant-height nc-AFM frequency shift image of 6-ZGNR. Reprinted with permission.[30] Copyright (2016) Macmillan Publishers Ltd. (d) Constant-height nc-AFM images of 9-AGNR.Reprinted with permission.[31] Copyright (2017) American Chemical Society.

bandgaps that are inversely proportional to their width.[28] Moreover, there are three subfamilies of AGNRs depending on the number of carbon atoms in their widths (N), and their bandgaps follow the order of $N = 3n + 1 > N = 3n \gg N = 3n + 2$.[28,29] Therefore, it is essential to make GQDs and GNRs with accurate edge structures and sizes/widths in order to achieve specific physical properties for fundamental investigations as well as for future applications.

GQDs and GNRs are mainly prepared by the so-called top-down methods as represented by lithographical patterning of graphene sheets,[19,32–36] but such methods have not demonstrated the possibility of making uniform and atomically precise structures that have the electronic properties as predicated by theory. On the other hand, large polycyclic aromatic hydrocarbons (PAHs), such as hexa-*peri*-hexabenzocoronene (HBC), can be regarded as nanographene or GQD for its nanoscale graphene-like structure consisting of hexagonal rings with sp^2 carbon atoms.[13,19,37,38] HBC can be facilely synthesized through oxidative cyclodehydrogenation of hexaphenylbenzene (HPB) as the precursor,[39] and this reaction can also be applied to tailor-made polyphenylene precursors, which allows for the bottom-up chemical synthesis of structurally defined GNRs in solution.[40,41] Moreover, bottom-up syntheses of GNRs were also achieved on metal surfaces under ultrahigh vacuum (UHV) conditions, where dihalide monomers are thermally polymerized via in-situ generation of diradical species, followed by the metal-surface-catalyzed cyclodehydrogenation, leading to GNRs.[40–42] Thus-formed GNRs can be directly characterized by modern surface science methods, and their atomically precise structures are demonstrated by high-resolution scanning tunneling microscope (STM) and atomic force microscope (AFM) (Figure 1c and d).[30,31,40,41,43,44]

Synthesis of novel PAHs and GNRs with unique structures and exploration of their properties as well as possible applications are the key driving forces of our research. We have thus devoted our efforts to development of unprecedented PAHs (chapters 2 and 3) and GNRs (chapter 4) as well as other related conjugated carbon nanostructures (chapter 5). Furthermore, edge functionalization of PAHs and GNRs enable further mod-

ulation of their properties (chapter 6). We have also explored new methods for on-surface synthesis of GNRs without the use of UHV that requires an expensive setup and limits the scalability of the synthesis (chapter 7). To this end, we have used an industry viable setup for chemical vapor deposition, allowing for simpler on-surface synthesis of GNRs over larger areas. In this account, we describe our recent achievements mainly during the last five years, highlighting our ideas and motivations, and discuss the prospects of our PAHs and GNRs. On the other hand, readers are advised to refer to previous review and account articles by us[19,40,41,44–46] and others[42,47–59] for more comprehensive descriptions of the field.

2. Synthesis of Novel PAHs with Zigzag Edges

During over 100 years of research history as pioneered by Scholl[60–62] and Clar,[63–65] numerous PAHs have been synthesized and reported, demonstrating varying optical and electronic properties depending on their chemical structures. After demonstration of the synthesis of HBC through the oxidative cyclodehydrogenation of HPB in 1995,[66] larger and larger PAHs, namely nanographenes, with armchair edges have been synthesized by applying this reaction to larger oligophenylene precursors.[39,41] The largest example synthesized to date is a hexagonal nanographene consisting of 222 sp^2 carbon atoms.[67] UV-vis absorption spectra revealed the lowering of the optical energy gap of such nanographenes as their size increases.[68] On the other hand, PAHs with zigzag edges, as represented by acenes,[69] periacenes,[70] anthenes,[71] and zethrenes[72] display unique physical and chemical properties, such as higher chemical reactivity, small optical gaps for relatively small sizes, and open-shell character, which are distinct from PAHs only with armchair edges.[69,71,73,74] For example, Kubo and co-workers reported syntheses of teranthene[75] and quarteranthene,[76] revealing their open-shell characters in ground state. In 2018, Feng[77] et al. and Wu[78] et al. independently achieved syntheses of peritetracene, also exhibiting open-shell biradical character. In the same year, Wu et al. further reported syntheses of a series of PAHs having four zigzag edges,[79] which displayed amplified spontaneous emission (ASE) and could be applied in lasers.[80] However, there are still a relatively limited number of PAHs having zigzag edges reported in the literature, and many of them suffer from low stability, prohibiting their in-depth studies and applications.

To this end, in 2016, we reported a π-extension of HBC by addition of four K-regions, leading to novel PAH **3** having a combination of armchair and zigzag edges (Figure 2).[81] The zigzag edges cannot be formed through the conventional oxidative cyclodehydrogenation, namely C-C bond formation between aryl groups that can only make a bay region, or an armchair edge. Therefore, we have pre-installed two zigzag edges in precursor **2** prior to the cyclodehydrogenation, through four-fold intramolecular alkyne cyclization[82] of precursor **1** (Figure 2). The low solubility of PAH **3** did not allow its characterization by NMR or single-crystal X-ray analysis. Nevertheless, the structure of **3** could be unambiguously verified by matrix-assisted laser desorption/ionization time-of-flight (MALDI-TOF) mass spectrometry (MS) and STM visualization as well as IR and Raman spectroscopy in combination with simulation by density functional theory (DFT) calculations, in collaboration with groups of Steven de Feyter and Matteo Tommasini. Moreover, the UV-vis spectrum exhibited a red-shifted absorption extending up to ~700 nm and DFT calculations indicated an energy gap of 2.5 eV between the highest occupied molecular orbital (HOMO) and the lowest unoccupied molecular orbital (LUMO). This value is 1.1 eV smaller than the HOMO–LUMO gap calculated for the pristine HBC, highlighting the notable effect of the four extra K-regions, forming the zigzag edges, on the electronic properties of HBC.

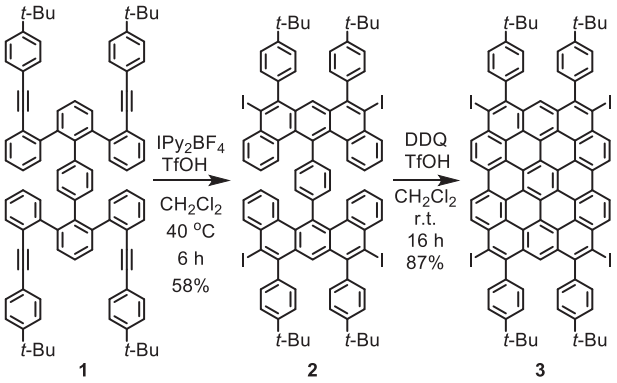

Figure 2. Synthesis of HBC **3** with four additional K-regions via precursor **2** with pre-installed zigzag edges. IPy_2BF_4: bis(pyridine)iodonium tetrafluoroborate; TfOH: triflic acid; DDQ: dichloro-5,6-dicyano-1,4-benzoquinone.

Moreover, in 2017, we reported another new PAH having a combination of armchair and zigzag edges, namely dibenzo[*hi*,*st*]ovalene (DBOV).[83] Similar to PAH **3**, the zigzag edges of DBOV cannot be formed upon the cyclodehydrogenation. Nevertheless, it is more challenging to design a precursor with pre-installed zigzag edges for DBOV. Synthesis of DBOV was thus carried out by "bridging" cove regions of fused bichrysene **9** to form zigzag edges in the final steps (Figure 3). The synthesis of fused bichrysene, having the same aromatic core structure as **9**, was pioneered by Chen and Liu.[84] For the preparation of the key intermediate **9**, bichrysene **5** was initially performed through platinum (Pt)-catalyzed cyclization of diaryldiacetylene **4** to afford bichrysene **5**, which was subsequently subjected to the oxidative cyclodehydrogenation (Figure 3a), using the synthetic method established by Chen and Liu.[84] However, the cyclodehydrogenation failed to afford **9** under different conditions, presumably due to the electron-withdrawing formyl groups. Therefore, we converted formyl groups of **5** to acetoxymethyl groups to afford **6**, which could be cyclized to fused bichrysene **7** through the cyclodehydrogenation (Figure 3a, blue arrows). After conversion of acetoxymethyl groups of **7** back to formyl groups to provide **9**, DBOV **10** with mesityl (Mes) groups could then be obtained by treatment of **9** with mesitylmagnesium bromide, and then $BBr_3 \cdot OEt_2$, followed by oxidation (Figure 3b). However, the total yield was only 2% through 12 steps.[85] To this end, we have more recently developed a more concise and efficient synthetic route through cyclization of diaryldiacetylene **4** with ICl, yielding iodinated bichrysene **8**, followed by photochemical cyclodehydroiodination[86] to afford fused bichrysene **9** (Figure 3a, red arrows).[87] Through this new route, **9** could be obtained in a gram scale, allowing for syntheses of various DBOV derivatives with

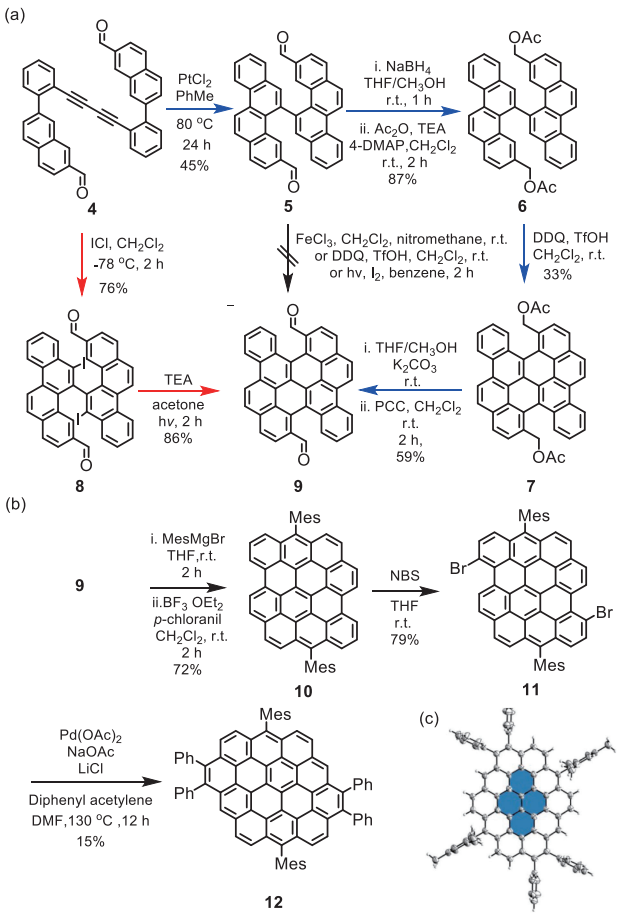

Figure 3. (a) Synthesis of fused bischrysene **9** through a sequence of ICl-promoted iodination-benzannulation and photochemical cyclodehydroiodination (red arrows) vs. the cyclodehydrogenation (blue arrows). (b) Synthesis of DBOV **10** and then circumpyrenes **12** via bromination and Pd-catalyzed benzannulation (c) Single-crystal structure of circumpyrene **12** (front view).[91] THF: tetrahydrofuran; DMF: *N*,*N*-dimethylformamide; TEA: triethylamine; NBS: *N*-bromosuccinimide; 4-DMAP: 4-dimethylaminopyridine; PCC: pyridinium chlorochromate; Ac_2O: Acetic anhydride.

different substituents, including dodecyl, 2,6-dimethylphenyl (DMEP), 2,3,4-tris(dodecyloxy)phenyl (TDOP), 4-trifluoromethylphenyl, and triisopropylsilylethynyl groups, in total yields of 23–41% over 7 steps.[87,88]

DBOV derivatives demonstrated strong red-light emission with high photoluminescence quantum yields (PLQY) of up to 89%. Moreover, ultrafast transient absorption analysis of DBOVs in collaboration with the group of Francesco Scotognella revealed a stimulated emission (SE), which indicated the applicability of DBOVs as an optical gain material, for example in laser and optical amplifier.[83,89,90] Although DBOVs showed aggregation-induced quenching of the fluorescence, blending of 1 wt% DBOV in polystyrene (PS) matrix allowed for solid-state emission and SE, leading to the observation of amplified stimulated emission (ASE) with a relatively low power threshold of ~60 μJcm^{-2}. DBOVs exhibited very high stability under ambient conditions and there was only a 30% decay after 30 min irradiation under air at a high laser fluence of 320 μJcm^{-2}. On the other hand, fluorescence correlation spectroscopy analysis, in collaboration with Thomas Basché, on isolated molecules of DBOV-DMEP embedded in Zeonex polymer film revealed single-photon emission, or photon-antibunching, indicating the potential of DBOV as a single-photon emitter, for example, for quantum optics.[87]

Furthermore, in collaboration with Mischa Bonn, we have revealed that DBOV **10** has blinking properties, which can be used for single-molecule localization microscoye (SMLM) that is a kind of super-resolution microscopy.[92] DBOV **10** exhibited the blinking time of 87 ms, which is about 1.3-fold longer than that of a standard organic dye, Alexa 647 (69 ms). Notably, DBOV **10** showed the blinking under any environment, even under air or inert atmosphere, in stark contrast to Alexa 647 and other organic dyes that require special buffer for the blinking that is essential for the SMLM applications. These results highlight the potential of DBOVs also for imaging applications, in particular for the bioimaging. To this end, we are currently working on syntheses of water-soluble DBOVs.

In the view of further functionalization as well as π-extension of DBOV, we have performed bromination of DBOV **10**, selectively affording brominated DBOV **11** (Figure 3b) as revealed by single-crystal X-ray analysis.[93] Besides introduction of different functional groups through transition-metal-catalyzed coupling reactions, we have further considered π-extension at the brominated bay regions of DBOV **11**, which would lead to circumpyrene.[91] Circumarenes are a subclass of PAHs that featured a central aromatic core surrounded by one outer layer of annulene, as represented by circumbenzene (coronene) and circumnaphthalene (ovalene). Circumanthracene was first reported by Diederich et al. in 1991[94] and more recently by Feng and his colleagues in 2018.[77] To our delight, palladium (Pd)-catalyzed benzannulation of **11** with diphenylacetylene afforded circumpyrene **12** (Figure 3b).[91] The structure of **12** could be unambiguously characterized by a combination of NMR, MALDI-TOF MS, and single-crystal X-ray diffraction analysis (Figure 3c), revealing its multi-zigzag-edged structure. **12** is the largest circumarene synthesized to date with pyrene as the core. Compared to the that of DBOV **10**, optical and electrochemical energy gaps of circumpyrene **12** were increased, which was in good agreement with (TD-)DFT calculations. This observation is also in line with Clar's aromatic sextet rule, since the number of Clar's sextets was increased from DBOV (four) to circumpyrene (five).

As higher homologues of bisanthene (perianthracene), corresponding to short segments of 4-ZGNR, syntheses of peritetracene and peripentacene were important targets in the field of PAHs. While syntheses of peritetracene derivatives were achieved independently by the groups of Feng[77] and Wu[78] in 2018 and an on-surface synthesis of peripentacene was demonstrated by Fischer, Crommie, and co-workers in 2015,[95] we have considered heteroatom-doped analogues of periacenes to enhance their stability as well as to modulate the physicochemical properties.[96] We initially attempted but failed in a synthesis of a peritetracene analogue with nitrogen-boron-nitrogen (NBN)-substituted zigzag edges, extending a previous synthesis of NBN-doped dibenzophenalene.[97] We subsequently worked on an oxygen-boron-oxygen (OBO)-doped peritetracene analogue **14**, and succeeded in its synthesis through oxi-

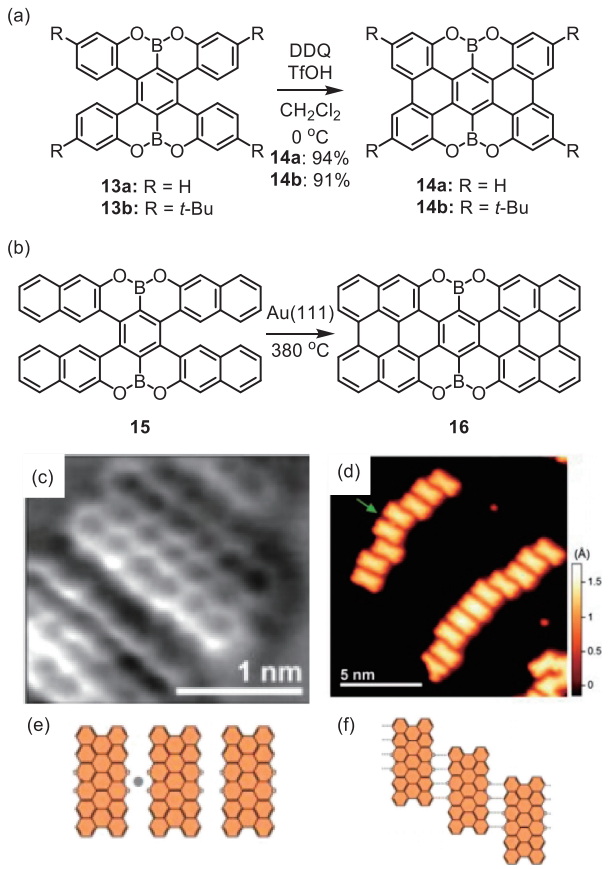

Figure 4. (a) Synthesis of OBO-doped peritetracene analogue **14** through cyclodehydrogenation of precursor **13**. (b) On-surface synthesis of OBO-doped perihexacene analogue **16** from precursor **15** on an Au(111) under UHV conditions. (c) nc-AFM image and (d) STM image of **16**. (e) Schematic representation of the abreast molecular assembly based on **16** (gray dot representing an occasional Au adatom). (f) Structure model of the self-assembly based on O···H hydrogen bonds (indicated by dotted lines). (c, d, e, f) Reproduced with permission.[100] Copyright (2017) American Chemical Society.

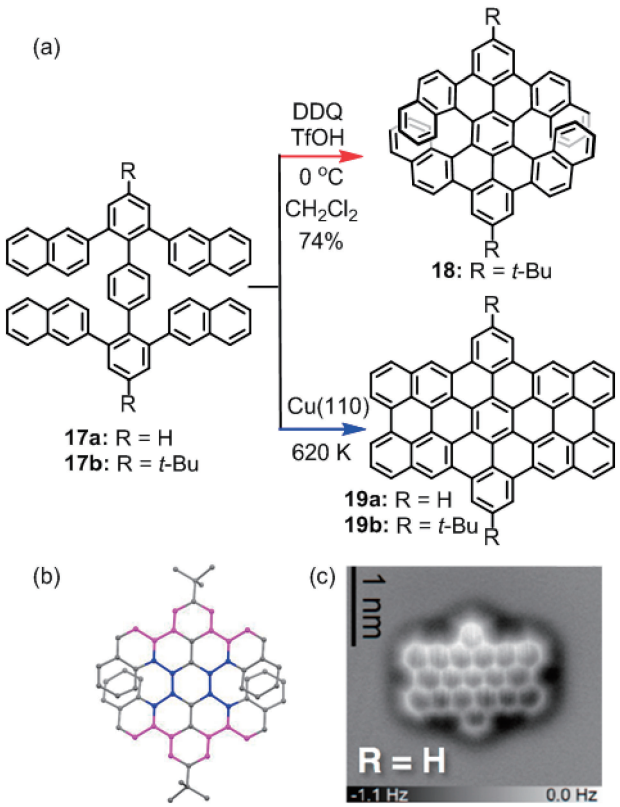

Figure 5. (a) Syntheses of double [7]carbohelicenes **18** in solution (Red arrow) and dibenzoperihexacene **19** on metal surfaces (Blue arrow) from tetranaphthyl-*p*-terphenyl **17**. (b) Single-crystal structures of **18**. Reproduced with permission.[104] Copyright (2017) Wiley Library. (c) AFM image of **19a**.[105]

dative cyclodehydrogenation of OBO-doped bistetracene **13**.[98] **14** exhibited high stability as well as interesting optical properties with sharp absorption and emission peaks and a small Stokes shift of 7 nm, reflecting its rigid aromatic core structure. It should be noted that Hatakeyama and co-workers also reported syntheses of OBO-doped bistetracenes, highlighting their double [5]helicene structure and succeeding in the optical resolution by introduction of *tert*-butyl groups to prevent the racemization.[99]

We have subsequently pursued a synthesis of a higher homologue, OBO-doped perihexacene **16** using OBO-doped bishexacene **15** as the precursor (Figure 4b).[100] DFT calculations indicated a HOMO-LUMO energy gap of 2.47 eV for **16**, 0.5 eV smaller than that of OBO-peritetracene **15** (2.97 eV). The oxidative cyclodehydrogenation of **16** in solution was not successful under various conditions. Nevertheless, we have then collaborated with the group of Roman Fasel to perform the cyclodehydrogenation of **15** on an Au(111) surface under UHV conditions, and clearly observed the formation of OBO-doped perihexacene **16** by high-resolution STM and nc-AFM after annealing at 370 °C (Figure 4c). Interestingly, both **15** and **16** displayed unique row-like self-assembly due to hydrogen bonding or coordination with a gold atom, involving the OBO-doped edges (Figure 4d–f), highlighting a potential of such heteroatom-doping for programming the self-assembly of nanographenes and GNRs on surface. We have more recently further extended the synthesis to OBO-doped chiral (4,1)-GNRs (Figure 9, see Chapter 4).

With a goal of synthesizing benzo-fused ZGNRs as novel low-bandgap GNRs[101] with presumably higher stability than that of pristine ZGNRs, we have designed benzo-fused perihexacene **19** (Figure 5) as a model structure corresponding to a short benzo-fused ZGNR. Such use of benzo-fused zigzag edges can also be considered as a strategy to stabilize the periacenes, in analogy to benzo-fused higher acenes that show improved stabilities.[102,103]

We have thus synthesized tetranaphthyl-*p*-terphenyl **17b** as a precursor of benzo-fused perihexacene **19b** and performed the oxidative cyclodehydrogenation reaction in solution. Initial MALDI-TOF MS analysis indicated that the cyclodehydrogenation could not be completed. Nevertheless, a single-crystal X-ray analysis unambiguously revealed an unexpectedly formation of benzo-fused double [7]helicene **18**,[104] which could be rationalized by the higher spin density at the α-position of

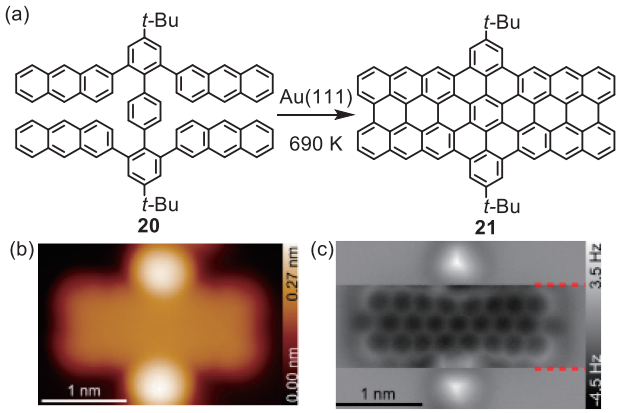

Figure 6. (a) Synthesis of dibenzoperioctacene **21** from tetraanthryl-*p*-terphenyl **20** on Au(111). (b) STM image and (c) AFM image **21**.[105]

the naphthyl group in the radical cation reaction intermediate of **17** (Figure 5, see also Chapter 3).[105]

While we are still trying to optimize the precursor structure and cyclodehydrogenation conditions to obtain benzo-fused perihexacene **19** in solution, we have collaborated with the group of Lifeng Chi to carry out on-surface cyclodehydrogenation of precursor **17b**.[105] Interestingly, the regioselectivity of the cyclodehydrogenation was completely altered by the effect of the metal surface, leading to formation of benzo-fused perihexacene **19b** via C-C bond formation at the β-positions of naphthyl groups. The formation of **19b** could be clearly validated by high-resolution STM and AFM visualizations on different metal surfaces, namely Au(111), Cu(111), and Cu(110). Nevertheless, relatively random intermolecular coupling was also observed, presumably due to removal of the *tert*-butyl groups, in-situ generating a highly reactive radical species. To this end, we have synthesized unsubstituted tetranaphthyl-*p*-terphenyl **17a**, which led to the formation of benzo-fused perihexacene **19a** without significant intermolecular coupling, with a yield of 56% on an Au(111) surface. HOMO-LUMO energy gaps of benzo-fused perihexacene **19a** and **19b** were estimated by scanning tunneling spectroscopy (STS) analyses to be both approximately 2.1 eV on Au(111) surfaces.

Moreover, we have further synthesized tetraanthryl-*p*-terphenyl **20** for a synthesis of a higher homologue of **19**, benzo-fused perioctacene **21** (Figure 6a). Annealing of **20** on Au(111) at ~420 °C successfully yielded benzo-fused perioctacene **21**, as revealed by STM and atomic-resolution nc-AFM analysis (Figure 5b, Figure 5c). STS analysis of **21** elucidated its HOMO-LUMO energy gap of 1.3 eV, demonstrating a significant lowering by 0.8 eV upon extension from benzo-fused perihexacene **19**. These results indicate the strength of the on-surface method for syntheses of such periacene analogues that are challenging to obtain in solution as well as highlight the possibility of drastically lowering the energy gap by extending to higher homologues.

3. Synthesis of Novel Double Helicenes

Helicenes are screw-shaped helical PAH consisting of *ortho*-fused benzene rings.[54,106] Synthesis of higher helicenes has been a continuous target in organic chemistry,[107] in view of

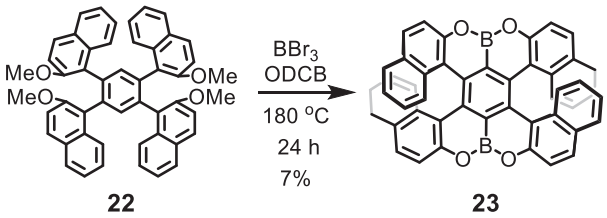

Figure 7. Synthesis of OBO-doped double [7]helicene **23** through a tandem demethylation–borylation reaction of precursor **22**. ODCB: *o*-dichlorobenzene.

their inherent chirality and various potential applications, for example, in asymmetric catalysis,[108] chiral optics,[109] and chiral sensing.[110] In 2015 Fujita and co-workers reported a synthesis of [16]helicene, having triple-layered structure, which is the highest helicene to date.[111] More recently, double helicenes, which possess two helicene moieties in one molecule, as well as multiple helicenes with more than two helicene moieties have attracted growing attention, in view of their unique properties such as enhanced structural distortion, multidimensional intermolecular interactions, and circularly polarized luminescence.[52,54,106] Double [5]helicene was initially reported by Clar et al. in 1959,[112] and later synthesized by Kamikawa et al in 2015.[113] In the same year, Itami and co-workers reported a synthesis of double [6]helicene,[114] and Hatakeyama and his colleagues synthesized boron-fused double [5]helicenes, showing ambipolar conductivity and CPL.[115] However, double and multiple helicenes have still remained underdeveloped.

During a synthesis of OBO-doped peritetracene **14** as described in Chapter 2, we were intrigued by the double [5]helicene structure of OBO-doped bistetracene **13**, which we observed in its single-crystal structure. Detailed characterizations and optical resolution of OBO-doped bistetracene as a double [5]helicene were nicely achieved and reported by Hatakeyama et al., through introduction of bulky *tert*-butyl groups to hinder the isomerization.[115] On the other hand, in parallel with the synthesis of OBO-doped bishexacene **15** (Figure 4), we carried out a synthesis of its isomer, OBO-doped double [7]helicene **23**.[116] By subjecting 1,2,4,5-tetrakis-(2-methoxynaphthalen-1-yl)benzene **22** to a tandem demethylation–borylation reaction, following our previous synthesis of OBO-doped bistetracene **13**, OBO-doped double [7]helicene **23** could be obtained, which was the first double [7]hetero-helicene consisting solely of six-membered rings (Figure 7). The substantial overlap between terminal benzene rings of **23** could be clearly illustrated by a single-crystal X-ray analysis. Separation of **23** by chiral high-performance liquid chromatography (HPLC) allowed for the optical resolution, and the circular dichroism (CD) spectra agreed well with the simulation by DFT calculations. There was no racemization even after heating at 200 °C, in line with a high DFT-calculated isomerization barrier of 45.1 kacl/mol.

On the other hand, during our attempts to synthesize benzo-fused perihexacene **19**, we unexpectedly obtained benzo-fused double [7]carbohelicene **18**, as described in Chapter 2, which became the first purely hydrocarbon double [7]helicene reported in the literature (Figure 5a).[104] The oxidative cyclodehydrogenation of tetranaphthyl-*p*-terphenyl **17b** selectively afforded **18** in 74% yield, in spite of the high structural strain and pos-

sibility of forming a planar product, benzo-fused perihexacene **19**. The single-crystal structure of **18** revealed overlapping of the terminal benzene rings as well as the maximum dihedral angle of 33.8° in the central benzene ring, which is one of the highest twisting deformations of a benzene ring. DFT calculations indicated the isomerization barrier of **18** to be 46.0 kcal/mol, which was comparable to that of OBO-doped double [7]helicene **23**. Notably, **18** displayed a fluorescence peak at 565 nm with a quantum yield of 34%, which is relatively high for helicene derivatives and interesting for applications in chiral optics.

We have further explored a synthesis of π-extended double helicenes based on the oxidative cyclodehydrogenation of tetraaryl-*p*-terphenyl precursors, and achieved a synthesis of π-extended double [7]helicene **25** having four pyrene subunits by using **24** as a precursor (Figure 8).[117] Compared with **18**, pyrene-fused double [7]carbohelicene **25** displayed considerable intra- and intermolecular π–π interactions, which was evidenced by single-crystal X-ray analysis. Interestingly, **25** exhibited a broad near-infrared emission (600 to 900 nm) and a large Stokes shift ($2.3 \times 10^3\,cm^{-1}$), which are distinct from **18**. We considered that this observation could be due to intramolecular excimer-like effect, which could be corroborated by ultrafast transient absorption spectroscopy in collaboration with the group of Francesco Scotognella. Additionally, the racemization barrier of **25** was predicated to be $46.0\,kcal \cdot mol^{-1}$ by DFT calculations, comparable to those of **18** and **23**.

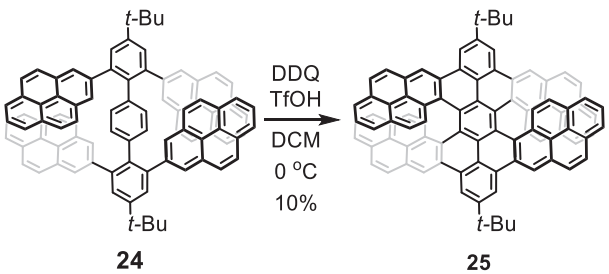

Figure 8. Synthesis of π-extended double [7]carbohelicene **25** through cyclodehydrogenation of precursor **24**.

4. Synthesis of Novel GNRs with Zigzag Edges

Through the bottom-up synthesis in solution,[40,41,44] on surfaces,[41] and in crystals,[118] a number of GNRs with different structures have been achieved during the last decade, including AGNRs with different widths ($N = 5$, 7, 8, 9, 13),[31,40,43,119–122] chevron-type GNRs with varying π-extended structures,[123–125] cove GNR,[126,127] ZGNR,[30] and chiral (3,1)-GNR[128] with a combination of zigzag and armchair edges. Heteroatom-doping of GNRs has also been demonstrated, such as boron (B)-doping[129,130] or B- and nitrogen (N)-co-doping[131] of 7-AGNR and N[132]- and/or sulfur (S)[133]-doping of the chevron-type GNRs. Furthermore, GNRs can be laterally fused to make wider GNRs (e.g., 14- and 21-AGNRs from 7-AGNR)[134] and heterojunctions of different GNR segments can be formed by partial lateral fusion or by using two different monomer precursors.[132,135,136] Nevertheless, most of the GNRs thus far synthesized have armchair edges and those with partly or fully zigzag edges were only limited to chiral (3,1)-GNR and 6-ZGNR.

After our previous syntheses of OBO-doped peritetracene **14** in solution and OBO-doped perihexacene **16** on a surface (Figure 4), we have considered extending these syntheses of OBO-doped nanographenes to OBO-doped GNRs.[137] We have thus designed dibrominated OBO-doped bistetracene **26** as a GNR precursor, which leads to OBO-doped chiral (4,1)-GNR **28** (Figure 9). After preparation of **26**, we carried out an on-surface synthesis on Au(111) under UHV in collaboration with the group of Roman Fasel. Precursor **26** could be polymerized to polymer **27** upon annealing at 200 °C, and further thermal treatment at 450 °C induced the cyclodehydrogenation, affording OBO-doped GNR **28** as the first GNR having an analogous structure of chiral (4,1)-GNR as well as the second B-doped GNR in the literature. The formation of OBO-doped GNR **28** could be unambiguously elucidated by visualization with nc-AFM (Figure 9b) as well as high-resolution STM (Figure 9c), which also displayed its relatively large average length of 61 nm. Moreover, the STM image of OBO-doped GNR **28** also revealed its unique self-assembly behavior, exhibiting lateral alignment of GNRs through hydrogen bonding at the OBO-substituted edges, which occurred in homochiral and hetero-

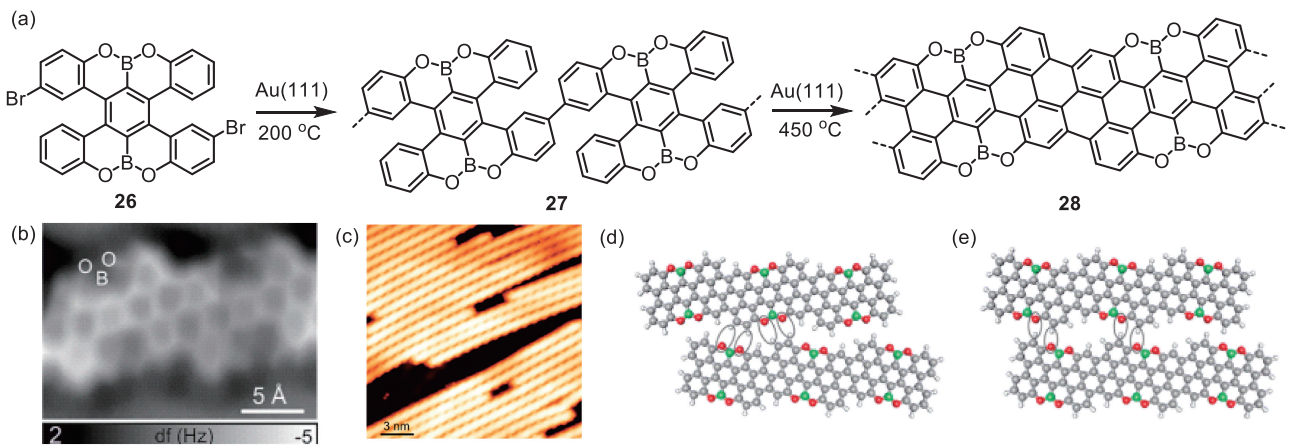

Figure 9. (a) Synthesis of OBO-doped chiral (4,1)-GNR **28** from monomer **26**. (b) Constant-height frequency-shift nc-AFM image and (c) STM overview of OBO-doped (4,1)-GNR **28** on Au(111). (d, e) DFT models showing interactions of **28** in heterochiral and homochiral configurations, respectively. Reproduced with permission.[137] Copyright (2018) American Chemical Society.

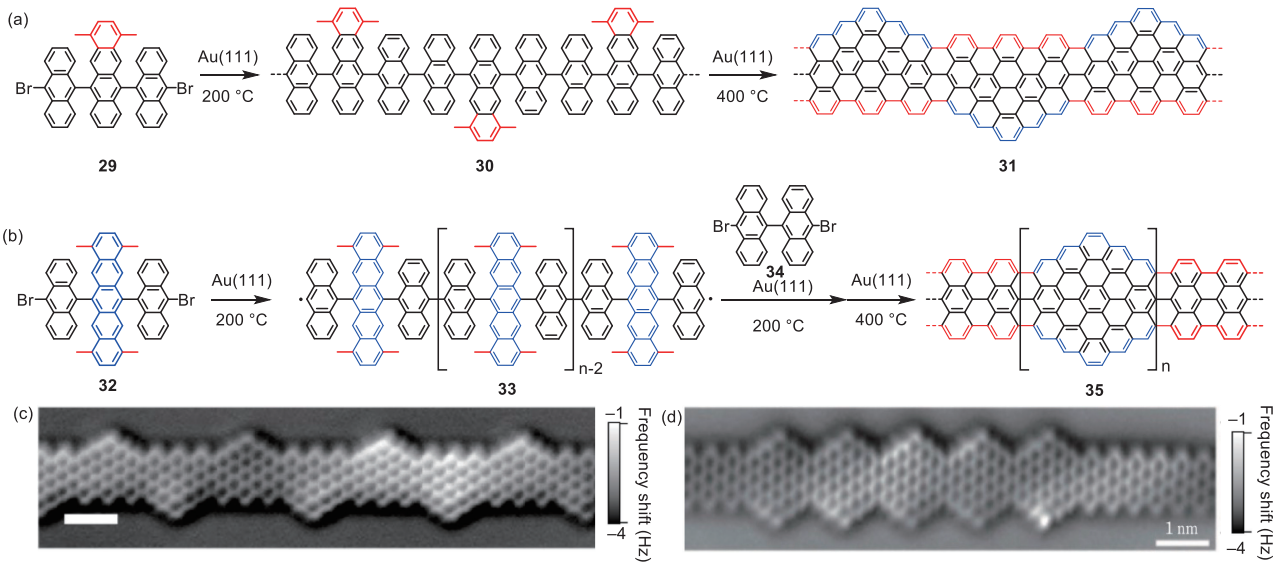

Figure 10. On-surface synthesis of (a) zigzag-extended 7-AGNR **31** and (b) heterojunction of pristine 7-AGNR and zigzag-extended 7-AGNR **35**. nc-AFM images of (c) **31** and (d) **35**. Reproduced with permission.[138] Copyright (2018) Macmillan Publishers Ltd.

chiral configurations (Figure 9d and e).

During the synthesis of 6-ZGNR, it was revealed that methyl groups can be used to form a zigzag edge in the on-surface synthesis.[30] Namely, methyl group positioned at a cove region can undergo oxidative cyclization against a neighboring benzene ring, "bridging" the cove to form a zigzag, which occurs upon annealing on a metal surface simultaneously with the cyclodehydrogenation. We considered further utilization of a methyl group for syntheses of novel GNRs having zigzag edges. We have thus designed precursor **29** having a dimethyltetracene core with two bromoanthryl units, which could also be seen as "insertion" of the dimethyltetracene unit in the structure of dibromobianthryl **34** that is used for a synthesis of 7-AGNRs (Figure 10a).[138] The methyl groups on the tetracene core were expected to form zigzag edges with the anthryl units. To our delight, an on-surface synthesis using precursor **29**, in collaboration with the group of Roman Fasel, successfully yielded GNR **31**, which has a structure based on a 7-AGNR backbone with zigzag-extended edges as clearly visualized by nc-AFM analysis (Figure 10c). Notably, STS analysis of GNR **31** revealed its bandgap of 0.65 eV, which is significantly smaller than that of the pristine 7-AGNR, namely 2.40 eV.

In analogy to precursor **29**, we have further designed and synthesized precursor **32** with a tetramethylpentacene core substituted with two bromoanthryl units (Figure 10b). Upon deposition and annealing on an Au(111) surface, precursor **32** could undergo polymerization and then cyclodehydrogenation with simultaneous formation of zigzag edges via the cyclization of the methyl groups, providing GNR **35** based on a 7-AGNR but with a fully zigzag-extended edge structure (Figure 10d).[138] Interestingly, theoretical studies by Oliver Gröning by tight-binding calculations indicated that GNR **35** has a topologically non-trivial electronic phase, based on the Su-Schrieffer-Heeger (SSH) model, and predicted that GNR **35** shows topological end states at the terminals. To avoid hybridization of this topological end state with another end state originating from the zigzag edge at the terminals,[139] a heterojunction of GNR **35** was fabricated by coupling with pristine 7-AGNR segments. Differential conductance (dI/dV) spectroscopy successfully revealed the predicted topological end state at the junctions with the pristine 7-AGNR segments, in perfect agreement with theoretical local density of states. These results highlighted the significant influence of the edge structures on the properties of GNRs and a new aspect of GNRs as potential topological materials.

5. On-Surface Synthesis of Indenofluorene Polymers

Indenofluorenes, consisting of a 6-5-6-5-6 fused-ring motif, have attracted interest in view of their inherent properties, such as antiaromaticity with 20 π-electrons,[140] biradical character,[141] and/or narrow energy gap,[142] as well as various potential applications, for example, in nonlinear optics and organic field-effect transistors.[143] In order to explore the further potential of the methyl group for expanding the repertoire of the on-surface synthesis, we synthesized 4,4″-dibromo-2,2″-dimethyl-*p*-terphenyl (**36**), which was expected to provide a polymer of indenofluorenes through the polymerization and the oxidative cyclization of methyl groups (Figure 11a).[144] Upon annealing of precursor **36** on an Au(111) surface at 200 °C, methylated poly(*p*-phenylene) (PPP) **37** could be obtained (Figure 11b), which was further heated at 350 °C to yield polymer **38** consisting of indeno[1,2-*b*]fluorene and indeno[2,1-*a*]fluorene units, as revealed by nc-AFM analysis (Figure 11c–e). PPP **37** was observed mostly in a conformation leading to indeno-[2,1-*a*]fluorene (Figure 11b), but indeno[1,2-*b*]fluorene was the main component of the resulting polymer **38**, indicating a flipping of methylphenylene subunits. This result could be rationalized by the fact that an indeno[2,1-*a*]fluorene unit induced 60° bending of the whole polymer chain, which was presumably unfavorable in comparison to the flipping, leading to a straight indeno[1,2-*b*]fluorene unit. Moreover, an energy gap of a polymer segment consisting of indeno[1,2-*b*]fluorene units could

be determined by an STS analysis to be 2.3 eV on Au(111).

While indeno[1,2-*b*]fluorene and indeno[2,1-*a*]fluorene are reported to have predominant closed-shell characters,[143] we have next aimed at an on-surface synthesis of indeno[2,1-*b*]-fluorene with an open-shell biradical character.[142] We have thus designed and synthesized 4,4″-dibromo-4′,6′-dimethyl-*m*-terphenyl **39** as the precursor, which can selectively yield indeno[2,1-*b*]fluorene unit (Figure 12a) without isomerization like in the case of precursor **36**.[145] Monomer **39** was thus sublimed onto an Au(111) surface, followed by radical polymerization at 150 °C to give methylated polyphenylene **40**. Subsequent thermal annealing at 250 °C induced the oxidative cyclization of methyl groups, and formation of polymer **41**, consisting of 10,12-dihydroindeno[2,1-*b*]fluorene units, could be confirmed by nc-AFM analysis (Figure 12b). Interestingly, when the sample was further annealed at 310 °C in an attempt to further oxidize polymer **41** to indenofluorene polymer **42**/**43**, we observed formation of porous ribbon **44**, consisting of tetraindenopyrene units (Figure 12d), through direct lateral fusion of generated polymers **42**/**43**. While the rest of the polymers remained as **41** at 310 °C, further annealing at 360–410 °C promoted the dehydrogenation of **41** to indenofluorene polymer **42**/**43**, as confirmed by nc-AFM visualization (Figure 12c). Notably, STS analyses of polymers **41** and **42**/**43**, as well as porous ribbon **44** revealed their markedly different bandgaps of 3.7, 0.4, and 2.2 eV, respectively, on Au(111) (Figure 12e). Moreover, ab initio calculations indicated anti-aromatic and open-shell characters of the low-bandgap indenofluorene polymer **42**/**43**, rendering it very interesting material for electronics and spintronics as well as for in-depth investigations of the magnetism in such carbon nanomaterials.

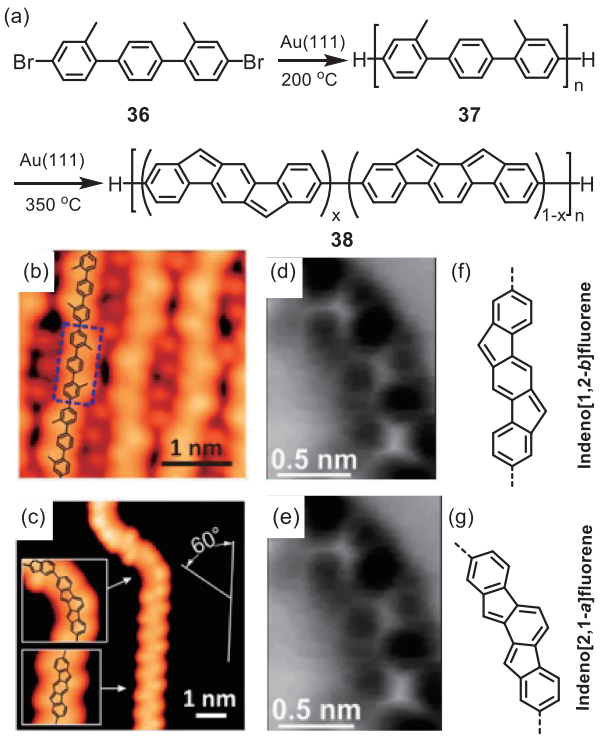

Figure 11. (a) On-surface synthesis of indenofluorene-based polymer **38**. STM images of (b) **37** and (c) **38**. (d, e) Constant-height frequency-shift nc-AFM images of **38**, displaying (d) indeno[2,1-*b*]fluorene and (e) indeno-[2,1-*a*]fluorene units with their chemical structures shown in panels f and g, respectively. Reproduced with permission.[144] Copyright (2019) American Chemical Society.

6. Edge Functionalization of GNRs

While it is often not simple to achieve PAHs and GNRs with new and different aromatic core structures or to introduce heteroatom-doping, their chemical and physical properties can be drastically modified and even tuned by substituting their peripheral positions with different functional groups, namely by edge functionalization.[41,68,146] To begin with, most of the large PAHs and GNRs synthesized in solution are substituted with bulky *tert*-butyl groups or long alkyl/alkoxyl chains, which can enhance their solubility and processability. In cases of PAHs, columnar self-assembly can be induced with nano-phase separation between the aromatic cores and peripheral chains, displaying discotic liquid crystalline characters.[88,147–150] Solution-synthesized GNRs can be liquid-phase processable

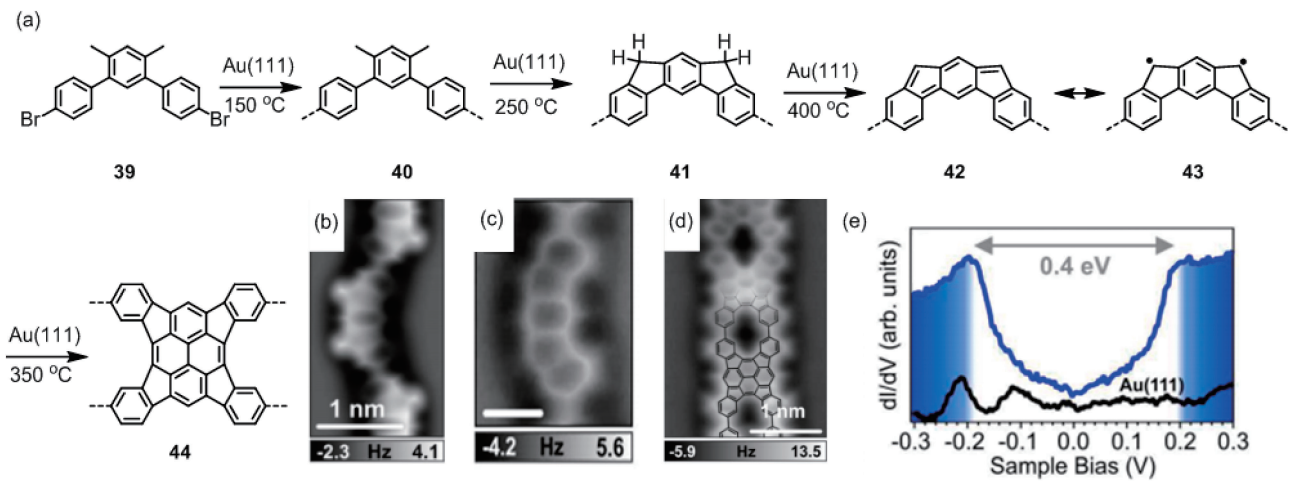

Figure 12. (a) On-surface synthesis of indenofluorene-based polymer **42**/**43** and porous ribbon **44**. Constant-height frequency-shift nc-AFM images of (b) **41**, (c) **43**, and (d) **44**. (e) dI/dV spectrum acquired on **42**/**43** (blue curve) and reference spectrum taken on the bare Au(111) surface (black curve). Reproduced with permission.[145] Copyright (2019) American Chemical Society.

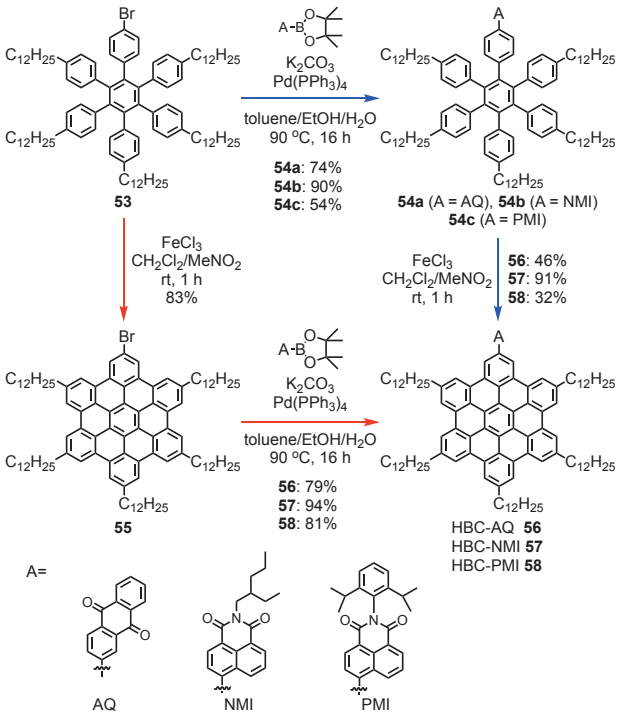

Figure 13. Syntheses of functionalized HBCs **56–58** through "pre-functionalization" (blue arrow) and "post-functionalization" (red arrow) routes.

with bulky substituents, in contract to on-surface-synthesized GNRs that can only be transferred as films.[40] On the other hand, mesityl groups are often used not only to increase the solubility, but also to kinetically protect highly reactive positions to isolate PAHs with otherwise instable aromatic core structures.[49,151] Furthermore, edge functionalization of PAHs typically with electron-donating and/or -withdrawing groups has been demonstrated to significantly affect their electronic and optical properties, for example inducing bathochromic shifts in the optical absorption spectra while reducing the HOMO-LUMO energy gaps and/or inducing intramolecular charge transfer.[152,153]

By using laterally extended monomer precursors, we have achieved solution syntheses of wider GNRs with the widths of up to ~2 nm, showing the lowering of the optical bandgap upon the lateral extension, in agreement with theoretical calculations.[154,155] Nevertheless, the dispersibility and thus processability of wider GNRs was compromised due to the extended aromatic core and resulting stronger aggregation. To this end, we consider different approaches to achieve lower-bandgap GNRs while preserving their processability, namely without making them wider. In addition to attempts to modulate the edge structure, we have designed GNRs **49–51** edge-functionalized with electron-withdrawing groups, namely anthraquinone (AQ), naphthalene monoimide (NMI), and perylene monoimide (PMI), respectively (Figure 13).[156]

We considered that edge functionalization with such electron-withdrawing groups could reduce the bandgap as well as lower the band energy levels, leading to n-type GNRs that were starkly underexplored. DFT calculations of GNRs **48a** and **49–51** were carried out in collaboration with David Beljonne, Jérôme Cornil, and their co-workers, which revealed that GNR-AQ **49** and GNR-PMI **51** have bandgaps of 1.69 and 1.94 eV, respectively, which are ~0.4 and ~0.1 eV smaller than that of GNR **48a** (2.05 eV) having only dodecyl groups (C12). On the other hand, the bandgap of GNR-NMI **50** (2.05 eV) was comparable to that of **48a**. Moreover, the energy levels of GNR-NMI **50** and GNR-PMI **51** were calculated to be 0.4–0.5 eV lower than those of GNR-C12 **48a**, indicating that this approach could indeed provide n-type GNRs.

Prior to the synthesis of GNRs **49–51** we had studied edge functionalization of HBC with AQ, NMI, and PMI units as model cases (Figure 13).[157] To investigate if these three functional groups can tolerate the oxidative cyclodehydrogenation conditions, we have applied two different pathways for the syntheses of the functionalized HBCs **56–58**, namely 1) "pre-functionalization" by coupling reaction before the cyclodehydrogenation and 2) "post-functionalization" by coupling after the cyclodehydrogenation (Figure 13). Notably, HBCs **56–58** could be synthesized by both the pre- and post-functionalization routes. MALDI-TOF MS analysis did not show any peak of possible byproduct with unclosed bond(s) or with formation of a five-membered ring between the functional group and the HBC core. Moreover, UV-vis absorption and emission spectra of HBCs **56–58** prepared through the two methods were effectively identical, proving that both methods can be employed for synthesizing HBCs **56–58** functionalized with AQ, NMI, and PMI groups.

Based on these results with HBC as the model, we performed syntheses of edge-functionalized GNRs **49–51** by using brominated polyphenylene precursor **46b**, which was prepared through an AB-type Diels–Alder polymerization of tetraphenylcyclopentadienone **45b** having one bromo and one dodecyl group (Figure 14).[156] Suzuki coupling of brominated precursor **46b** and corresponding boronic esters proceeded efficiently to provide functionalized precursors **47a–c**, which could be validated by MALDI-TOF MS analysis. Edge-functionalized GNRs **49–51** were then obtained through the oxidative cyclodehydrogenation of **47a–c**, respectively, and characterized by a combination of IR, Raman, and UV-Vis absorption spectroscopy and XPS analysis. UV-vis absorption spectra indicated that the optical bandgaps of GNRs **49–51** were comparable to that of GNR-C12 **48a**, distinct from the electronic bandgaps calculated by DFT. This result agreed with optical spectra simulated by TD-DFT calculations while our attempts to reveal the differences in the electronic bandgaps of GNRs **49–51** are still ongoing.

On the other hand, in collaboration with Boya Radha, we have observed an intriguing modulation of the self-assembly behavior upon the edge functionalization. While GNR-AQ **49** and GNR-NMI **50** formed domains of GNRs aligned parallel upon deposition on graphite surfaces (Figure 14b and c, respectively), similar to GNR-C12 **48a**, GNR-PMI **51** demonstrated networks of rectangularly crossed GNRs and GNR bundles, as revealed by AFM imaging (Figure 14d). We assume that the extended aromatic core of the PMI unit interacted with another GNR, drastically changing the self-assembled structure.

Moreover, in collaboration with Lapo Bogani, we have conceived edge functionalization of GNRs with organic radicals, which can induce magnetic edge states by spin injection from

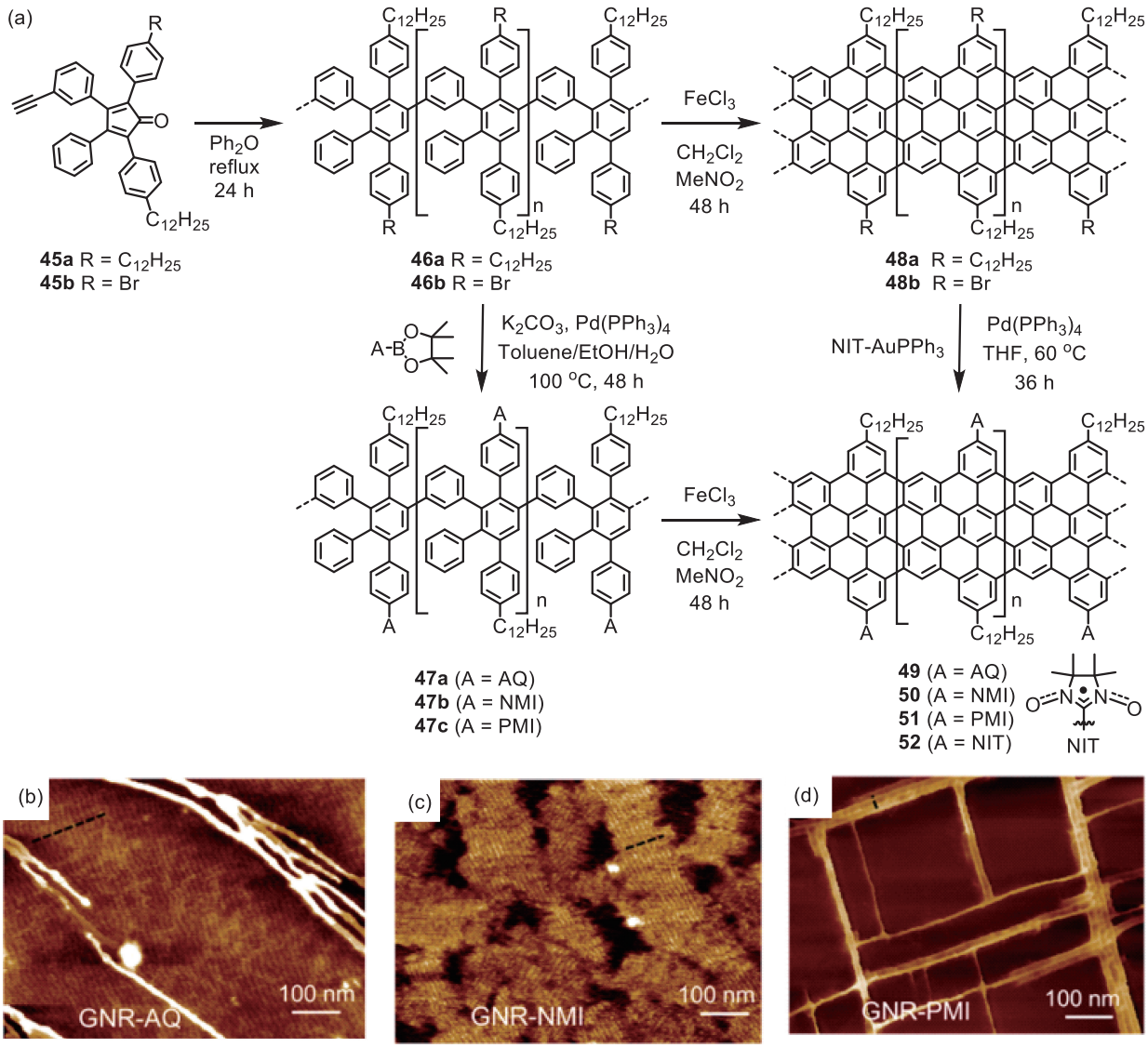

Figure 14. (a) Synthetic protocol for the edge-functionalization of GNRs with AQ, NMI, PMI and NIT units. AFM height image of (b) GNR-AQ **49**, (c) GNR-NMI **50**, and (d) GNR-PMI **51**.[156]

the peripheral radicals into the GNR core.[158] This approach can be an alternative to the use of GNRs having the edge state, which are generally unstable like ZGNRs and have only been studied under UHV. We have thus introduced nitronyl-nitroxide radicals (NIT) to the edge of GNRs by using GNR-Br **48b** bearing bromo groups and through a Pd-catalyzed cross-coupling reaction using an Au-complex of NIT (Figure 14a), which was developed by Okada and co-workers.[159] Spin density calculations of GNR-NIT **52** indicated a spin injection from the NIT units into the GNR core, inducing a magnetic state delocalized over the GNR, which could be evidenced by electron spin resonance (ESR) spectroscopy in collaboration with Lapo Bogani. Unlike the unstable ZGNRs, GNR-NIT **52** could be obtained as powder and handled under air, marking the superiority of GNR-NIT **52** in terms of stability. Moreover, the delocalized spin state over the GNR core and the other spin state localized on the NIT units could potentially serve as Qubits for the development of quantum computers.

7. Exploration of New Methods for On-Surface Synthesis of GNRs

The on-surface synthesis of GNRs under UHV conditions allowed the formation and visualization of atomically precise GNRs with various structures having armchair, zigzag, and cove edges and their combinations as well as those with heteroatom doping. However, the use of UHV conditions requires an elaborate and expensive setup and relatively long sample preparation time while the obtained samples are typically limited to areas smaller than 1 cm^2. The UHV conditions are advantageous to suppress possible side reactions by eliminating oxygen, water, and other possible contaminants from the air, but the on-surface reaction itself could be carried out also without the vacuum provided that the monomers, intermediates, and the resulting GNRs are stable under the applied condition. To this end, Nakae, Sakaguchi, and their co-workers have reported on-surface syntheses of AGNRs with different widths

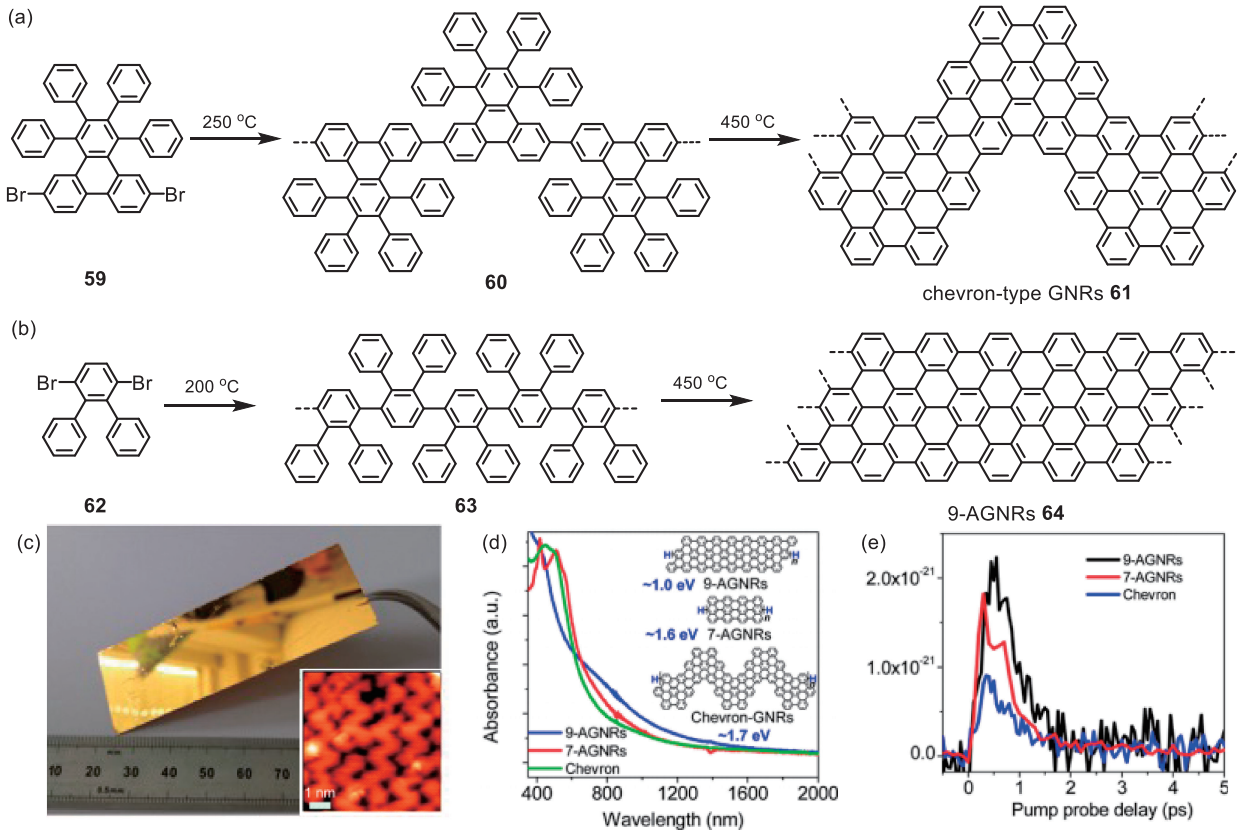

Figure 15. Syntheses of (a) chevron-type GNR **61** and (b) 9-AGNR **64** under the CVD conditions. (c) Photograph of a 25 × 75 mm^2 Au/mica plate, on which a GNR film could be grown. Inset shows an STM image of chevron-type GNR **61**. Reproduced with permission.[162] Copyright (2016) American Chemical Society. (d) UV-vis-NIR absorption spectra of chevron-type GNR **61**, 9-AGNR **64**, as well as 7-AGNR prepared under the CVD conditions. The inset shows the chemical structures of the GNRs and their optical bandgaps. (e) Comparative study of THz photoconductivity of the three different GNRs. (c, d) Reprinted with permission.[163] Copyright (2017) American Chemical Society.

($N = 5$, 7, and 9) using their chemical vapor deposition (CVD) setup that is viable to industrial production.[160,161]

We have independently worked on the on-surface synthesis with a CVD setup, initially using 6,11-dibromo-1,2,3,4-tetraphenyltriphenylene (DBTT **59**) as the precursor to make chevron-type GNR **61** (Figure 15a).[162] DBTT **59** was thus sublimed onto an Au/mica substrate (Figure 15c) placed inside a tube furnace under a flow of argon and hydrogen, followed by annealing at 250 °C for the polymerization, and then at 450 °C for the cyclodehydrogenation. Notably, polymer **60** could be analyzed by MALDI-TOF MS directly on the gold surface, providing new evidence for the formation of polymer **60**, which was not available for the UHV-grown samples. Moreover, UHV STM analyses of polymer **60** and GNR **61** in collaboration with Carlos-Andres Palma and Johannes V. Barth clearly demonstrated their precise structures (Figure 15c, inset), comparable to those fabricated under UHV conditions. GNRs prepared on Au/mica can be transferred onto another substrate by removing mica and dissolving gold, with or without a support of polymer like PMMA.[160,161,164] Field-effect transistor device studies using transferred films of GNR **61**, in collaboration with Chongwu Zhou, exhibited high current on/off ratios of up to 6000.[162] Additionally, the CVD method allowed fabrication of GNR films over the area of 25 × 75 mm^2 (Figure 15c), which could potentially be further extended by using a larger furnace. This result indicates the high scalability of this method, which has a potential for industrial applications.

We have also confirmed a preparation of high-quality 7-AGNR by this CVD method,[162] and then attempted a synthesis of 9-AGNR with lower bandgap using 3′,6′-dibromo-1,1′:2′,1″-terphenyl (**DBTP**) as the precursor (Figure 14b).[162] The successful synthesis of 9-AGNR **64** could be validated by Raman spectroscopy, displaying a spectrum in perfect agreement with that of 9-AGNR **64** prepared under the UHV conditions. The optical band gap of obtained 9-AGNR **64** was examined by UV-Vis-NIR absorption spectroscopy by transferring multiple layers of the 9-AGNR film onto a transparent substrate, achieving a sufficient optical density. 9-AGNR displayed a broad absorption with an onset at ~1185 nm, corresponding to an optical bandgap of ~1.0 eV, which was smaller than those of the chevron-type GNR **61** (~1.7 eV) and 7-AGNR (~1.6 eV) (Figure 14d). Time-resolved THz spectroscopy studies in collaboration with Mischa Bonn's group revealed higher photoconductivity of 9-AGNR **64** in comparison to the chevron-type GNR **61** and 7-AGNR (Figure 15e), and an intrinsic charge-carrier mobility of 9-AGNR **64** could be estimated to be ~350 $cm^2 \cdot V^{-1} \cdot s^{-1}$, suggesting a potential of the CVD-grown 9-AGNR **64** for transistor device applications.

Furthermore, we have subsequently carried out a synthesis of 5-AGNRs through the CVD method, using dibromoperylene **65**

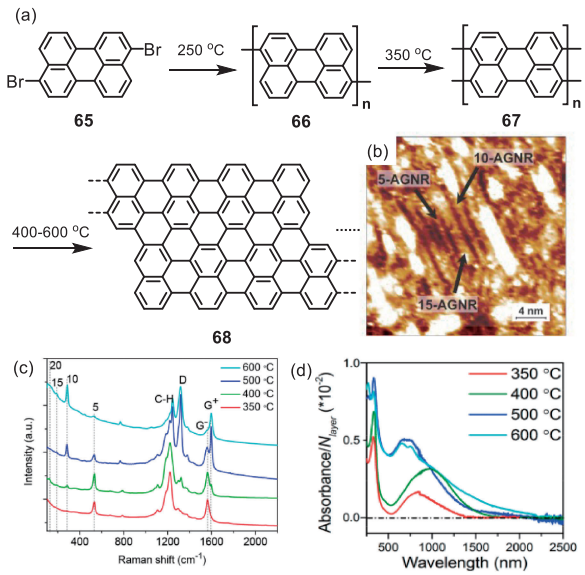

Figure 16. (a) CVD-based synthesis of 5-AGNR **67** and its lateral fusion to wider GNRs, including 10- and 15-AGNRs. (b) STM image showing the formation of broader GNRs at 600 °C ($I_{set} = 200$ pA, $V_{bias} = -0.4$ V). (c) Raman spectra of AGNRs annealed at different temperature. (d) UV–vis-NIR absorption spectra of samples annealed at different temperatures.[165]

and the precursor (Figure 16a).[165] The formation of 5-AGNRs could be verified by observation of a radial breathing-like model (RBLM) signal at 532 cm^{-1} in the Raman spectrum in agreement with theoretical calculations.[166] Samples prepared by annealing at 350 and 400 °C displayed absorption maxima at 900 and 1000 nm, respectively, in their UV-Vis-NIR spectra, in line with the low bandgap of 5-AGNR and suggesting that longer 5-AGNRs were obtained at higher temperature.

Interestingly, when we annealed the sample at 500 °C, we observed significant attenuation of the RBLM signal at 532 cm^{-1} originating from 5-AGNR and appearance of another RBLM peak at 285 cm^{-1} corresponding to 10-AGNR (Figure 16c). This result indicated lateral fusion of 5-AGNRs into 10-AGNRs, which could be further confirmed by STM visualization and UV-vis absorption spectroscopy (Figure 16b and d). UV-vis-NIR spectrum of the sample annealed at 500 °C displayed new blue-shifted peaks at 650 and 750 nm, which agreed very well with theoretical optical transitions of 10-AGNR predicated by GW-BSE calculations.[167] THz photoconductivity studies in collaboration with Mischa Bonn's group revealed lower conductivity of the sample annealed at 500 °C compared with those of samples at 350 and 400 °C in line with the theoretical prediction that the conductivity of GNRs is inversely proportional to their bandgaps.[21] Moreover, a sample annealed at 600 °C exhibited broadened UV–vis-NIR absorption extending up to about 2250 nm, which suggested formation of even wider AGNRs such as 15-AGNR and 20-AGNR (Figure 15d). Whereas RBLM peaks of 15- and 20-AGNR were not obvious at excitation wavelength of 785 nm, a clear signal corresponding to 15-AGNR could be clearly observed by excitation at 488 nm. These results demonstrate that lateral fusion can allow for syntheses of GNRs with different properties from the same precursor and the absorption over 2000 nm can be interesting for infrared sensing application.

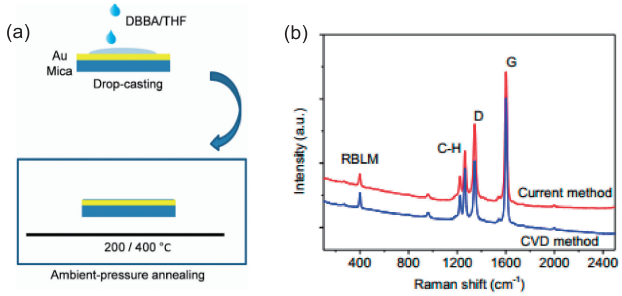

Figure 17. (a) Schematic illustration of GNR synthesis without thermal sublimation, that is through solution processing of monomers. (b) Raman spectra of 7-AGNRs prepared through the CVD and solution-processing methods. Reproduced with permission.[168] Copyright (2017) The Chemical Society of Japan.

For on-surface synthesis under UHV and CVD conditions, the monomer precursors need to be deposited by thermal and/or vacuum sublimation, which consumes a large amount of energy and precludes the use of thermally unstable and/or large monomers that cannot be sublimed. To address this problem, we have attempted an on-surface synthesis through solution processing of monomers without sublimation, followed by thermally induced polymerization and cyclodehydrogenation (Figure 16a).[168] To our delight, when we applied this method to monomer precursors **34** and **59**, 7-AGNR and chevron-type GNR **61** could be successfully obtained, which could be confirmed by Raman spectroscopy studies showing identical spectra for the GNRs prepared through the thermal sublimation and solution-processing of monomers (Figure 17b). These results constitute an important step forward to the practical application of such GNRs.

8. Conclusion

We have developed PAHs and GNRs with novel structures with an emphasis on the incorporation of zigzag edges, which induced intriguing properties such as strong red fluorescence and stimulated emission in DBOVs as well as topological electronic states in a zigzag-edge-extended 7-AGNR. We have also explored π-extended and OBO-doped double [7]helicenes, showing high conformational stabilities and intriguing optical properties. On the other hand, we have achieved edge-functionalization of GNRs, leading to modulation of the electronic properties and self-assembly behavior. Further, introduction of spin-bearing organic radicals on the peripheries of GNRs induced magnetic state over their aromatic cores through the spin delocalization. In parallel, we have developed simpler methods for the on-surface synthesis of GNRs using a CVD setup, without the use of UHV, allowing for simpler and scalable fabrication of GNR films. While we further explore syntheses of PAHs and GNRs with novel structures and properties, especially further incorporation of zigzag edges, heteroatoms, and/or helical structures, as well as edge-functionalization with unique chromophores, we in parallel investigate potential applications of PAHs and GNRs in various fields. For example, we explore the application of DBOV in organic lasers well as

single-photon emitters. We have also revealed that DBOV can serve as highly stable dye suitable for super-resolution microcopy, and are currently pursuing syntheses of water-soluble derivatives and further functionalization for bioimaging and biomedical applications. On the other hand, we are investigating fabrication of micro-supercapacitors based on GNRs prepared under the CVD conditions, and current results indicate excellent volumetric capacitance and very high power density. These results highlight the significance of synthesizing PAHs and GNRs with novel structures, which can lead to potential applications not only in electronic and optoelectronic devices, but also other fields, such as spintronics, energy storage, bioimaging, and biomedicine.

We acknowledge all of our distinguished collaborators and dedicated colleagues who enabled the achievements described in this article. We appreciate the financial support from the Max Planck Society, EU Project MoQuaS (FP7 FET-ICT-2013-10 610449), Graphene Flagship (No. CNECT-ICT-604391), the Marie Curie ITN project iSwitch (GA No. 642196), ERC-Adv.-Grant 267160 (NANOGRAPH), the Office of Naval Research BRC Program (molecular synthesis and characterization), DFG Priority Program SPP 1459 and the Alexander von Humboldt Foundation.

Dedicated to Professor Eiichi Nakamura on the occation of his 70th birthday.

References

1 K. S. Novoselov, A. K. Geim, S. V. Morozov, D. Jiang, Y. Zhang, S. V. Dubonos, I. V. Grigorieva, A. A. Firsov, *Science* **2004**, *306*, 666.
2 N. O. Weiss, H. L. Zhou, L. Liao, Y. Liu, S. Jiang, Y. Huang, X. F. Duan, *Adv. Mater.* **2012**, *24*, 5782.
3 Y.-M. Lin, C. Dimitrakopoulos, K. A. Jenkins, D. B. Farmer, H.-Y. Chiu, A. Grill, P. Avouris, *Science* **2010**, *327*, 662.
4 X. Yang, C. Cheng, Y. Wang, L. Qiu, D. Li, *Science* **2013**, *341*, 534.
5 K. N. Chen, Q. R. Wang, Z. Q. Niu, J. Chen, *J. Energy Chem.* **2018**, *27*, 12.
6 M. Burghard, H. Klauk, K. Kern, *Adv. Mater.* **2009**, *21*, 2586.
7 D. M. Sun, C. Liu, W. C. Ren, H. M. Cheng, *Small* **2013**, *9*, 1188.
8 C. Chung, Y. K. Kim, D. Shin, S. R. Ryoo, B. H. Hong, D. H. Min, *Acc. Chem. Res.* **2013**, *46*, 2211.
9 Y. Q. Yang, A. M. Asiri, Z. W. Tang, D. Du, Y. H. Lin, *Mater. Today* **2013**, *16*, 365.
10 N. Chauhan, T. Maekawa, D. N. S. Kumar, *J. Mater. Res.* **2017**, *32*, 2860.
11 I. Meric, M. Y. Han, A. F. Young, B. Ozyilmaz, P. Kim, K. L. Shepard, *Nat. Nanotechnol.* **2008**, *3*, 654.
12 F. Schwierz, *Nat. Nanotechnol.* **2010**, *5*, 487.
13 K. Müllen, *ACS Nano* **2014**, *8*, 6531.
14 S. V. Rajagopal, K. M. Fujiwara, R. Senaratne, K. Singh, Z. A. Geiger, D. M. Weld, *Ann. Phys.* **2017**, *529*, 1700008.
15 A. Celis, M. N. Nair, A. Taleb-Ibrahimi, E. H. Conrad, C. Berger, W. A. de Heer, A. Tejeda, *J. Phys. D: Appl. Phys.* **2016**, *49*, 143001.
16 R. Rieger, K. Müllen, *J. Phys. Org. Chem.* **2010**, *23*, 315.
17 M. Bacon, S. J. Bradley, T. Nann, *Part. Part. Syst. Charact.* **2014**, *31*, 415.
18 S. Kim, S. W. Hwang, M.-K. Kim, D. Y. Shin, D. H. Shin, C. O. Kim, S. B. Yang, J. H. Park, E. Hwang, S.-H. Choi, G. Ko, S. Sim, C. Sone, H. J. Choi, S. Bae, B. H. Hong, *ACS Nano* **2012**, *6*, 8203.
19 X.-Y. Wang, A. Narita, K. Müllen, *Nat. Rev. Chem.* **2017**, *2*, 0100.
20 L. A. Ponomarenko, F. Schedin, M. I. Katsnelson, R. Yang, E. W. Hill, K. S. Novoselov, A. K. Geim, *Science* **2008**, *320*, 356.
21 B. Obradovic, R. Kotlyar, F. Heinz, P. Matagne, T. Rakshit, M. D. Giles, M. A. Stettler, D. E. Nikonov, *Appl. Phys. Lett.* **2006**, *88*, 142102.
22 J. Y. Wang, R. Q. Zhao, M. M. Yang, Z. F. Liu, Z. R. Liu, *J. Chem. Phys.* **2013**, *138*, 084701.
23 K. Nakada, M. Fujita, G. Dresselhaus, M. S. Dresselhaus, *Phys. Rev. B: Condens. Matter* **1996**, *54*, 17954.
24 S. E. Stein, R. L. Brown, *J. Am. Chem. Soc.* **1987**, *109*, 3721.
25 J. R. Dias, *J. Phys. Org. Chem.* **2002**, *15*, 94.
26 M. Mukhopadhyay, B. Pandey, S. K. Pati, *Phys. Rev. Appl.* **2016**, *6*, 044014.
27 G. Z. Magda, X. Z. Jin, I. Hagymasi, P. Vancso, Z. Osvath, P. Nemes-Incze, C. Y. Hwang, L. P. Biro, L. Tapaszto, *Nature* **2014**, *514*, 608.
28 L. Yang, C.-H. Park, Y.-W. Son, M. L. Cohen, S. G. Louie, *Phys. Rev. Lett.* **2007**, *99*, 186801.
29 Y.-W. Son, M. L. Cohen, S. G. Louie, *Phys. Rev. Lett.* **2006**, *97*, 216803.
30 P. Ruffieux, S. Wang, B. Yang, C. Sánchez-Sánchez, J. Liu, T. Dienel, L. Talirz, P. Shinde, C. A. Pignedoli, D. Passerone, T. Dumslaff, X. Feng, K. Müllen, R. Fasel, *Nature* **2016**, *531*, 489.
31 L. Talirz, H. Söde, T. Dumslaff, S. Wang, J. R. Sanchez-Valencia, J. Liu, P. Shinde, C. A. Pignedoli, L. Liang, V. Meunier, N. C. Plumb, M. Shi, X. Feng, A. Narita, K. Müllen, R. Fasel, P. Ruffieux, *ACS Nano* **2017**, *11*, 1380.
32 M. C. Lemme, D. C. Bell, J. R. Williams, L. A. Stern, B. W. H. Baugher, P. Jarillo-Herrero, C. M. Marcus, *ACS Nano* **2009**, *3*, 2674.
33 A. N. Abbas, G. Liu, B. Liu, L. Zhang, H. Liu, D. Ohlberg, W. Wu, C. Zhou, *ACS Nano* **2014**, *8*, 1538.
34 X. Li, X. Wang, L. Zhang, S. Lee, H. Dai, *Science* **2008**, *319*, 1229.
35 L. Tapaszto, G. Dobrik, P. Lambin, L. P. Biro, *Nat. Nanotechnol.* **2008**, *3*, 397.
36 J. Bai, X. Duan, Y. Huang, *Nano Lett.* **2009**, *9*, 2083.
37 L. Chen, Y. Hernandez, X. Feng, K. Müllen, *Angew. Chem., Int. Ed.* **2012**, *51*, 7640.
38 X. Yan, B. Li, L.-s. Li, *Acc. Chem. Res.* **2013**, *46*, 2254.
39 J. Wu, W. Pisula, K. Müllen, *Chem. Rev.* **2007**, *107*, 718.
40 A. Narita, Z. Chen, Q. Chen, K. Müllen, *Chem. Sci.* **2019**, *10*, 964.
41 A. Narita, X. Y. Wang, X. L. Feng, K. Müllen, *Chem. Soc. Rev.* **2015**, *44*, 6616.
42 L. Talirz, P. Ruffieux, R. Fasel, *Adv. Mater.* **2016**, *28*, 6222.
43 J. Cai, P. Ruffieux, R. Jaafar, M. Bieri, T. Braun, S. Blankenburg, M. Muoth, A. P. Seitsonen, M. Saleh, X. Feng, K. Müllen, R. Fasel, *Nature* **2010**, *466*, 470.
44 A. Narita, X. Feng, K. Müllen, *Chem. Rec.* **2015**, *15*, 295.
45 I. C. Y. Hou, Y. B. Hu, A. Narita, K. Müllen, *Polym. J.* **2018**, *50*, 3.
46 N. Richter, Z. P. Chen, M. L. Braatz, F. Musseau, N. E.

Weber, A. Narita, K. Müllen, M. Kläui, *Ann. Phys.* **2017**, *529*, 1700051.
47 Y. Segawa, H. Ito, K. Itami, *Nat. Rev. Mater.* **2016**, *1*, 15002.
48 P. H. Jacobse, M. E. Moret, R. Gebbink, I. Swart, *Synlett* **2017**, *28*, 2509.
49 M. Stepien, E. Gonka, M. Zyla, N. Sprutta, *Chem. Rev.* **2017**, *117*, 3479.
50 R. Dorel, A. M. Echavarren, *Acc. Chem. Res.* **2019**, *52*, 1812.
51 M. Grzybowski, B. Sadowski, H. Butenschon, D. T. Gryko, *Angew. Chem., Int. Ed.* **2019**, doi:10.1002/anie.201904934.
52 C. Q. Li, Y. Yang, Q. Miao, *Chem.—Asian J.* **2018**, *13*, 884.
53 S. H. Pun, Q. Miao, *Acc. Chem. Res.* **2018**, *51*, 1630.
54 K. Kato, Y. Segawa, K. Itami, *Synlett* **2019**, *30*, 370.
55 E. von Grotthuss, A. John, T. Kaese, M. Wagner, *Asian J. Org. Chem.* **2018**, *7*, 37.
56 E. M. Muzammil, D. Halilovic, M. C. Stuparu, *Commun. Chem.* **2019**, *2*, 58.
57 M. A. Majewski, M. Stepien, *Angew. Chem., Int. Ed.* **2019**, *58*, 86.
58 I. Pozo, E. Guitian, D. Perez, D. Pena, *Acc. Chem. Res.* **2019**, *52*, 2472.
59 H. Zhylitskaya, M. Stepien, *Org. Chem. Front.* **2018**, *5*, 2395.
60 R. Scholl, C. Seer, *Justus Liebigs Ann. Chem.* **1912**, *394*, 111.
61 R. Scholl, C. Seer, *Ber. Dtsch. Chem. Ges.* **1922**, *55*, 330.
62 R. Scholl, C. Seer, R. Weitzenböck, *Ber. Dtsch. Chem. Ges.* **1910**, *43*, 2202.
63 E. Clar, D. G. Stewart, *J. Am. Chem. Soc.* **1953**, *75*, 2667.
64 E. Clar, J. F. Stephen, *Tetrahedron* **1965**, *21*, 467.
65 E. Clar, W. Schmidt, *Tetrahedron* **1979**, *35*, 2673.
66 A. Stabel, P. Herwig, K. Müllen, J. P. Rabe, *Angew. Chem., Int. Ed. Engl.* **1995**, *34*, 1609.
67 C. D. Simpson, J. D. Brand, A. J. Berresheim, L. Przybilla, H. J. Räder, K. Müllen, *Chem.—Eur. J.* **2002**, *8*, 1424.
68 Y.-Z. Tan, B. Yang, K. Parvez, A. Narita, S. Osella, D. Beljonne, X. Feng, K. Müllen, *Nat. Commun.* **2013**, *4*, 2646.
69 Z. Sun, Q. Ye, C. Chi, J. Wu, *Chem. Soc. Rev.* **2012**, *41*, 7857.
70 M. Watanabe, K.-Y. Chen, Y. J. Chang, T. J. Chow, *Acc. Chem. Res.* **2013**, *46*, 1606.
71 T. Kubo, *Chem. Lett.* **2015**, *44*, 111.
72 Z. Sun, Z. Zeng, J. Wu, *Acc. Chem. Res.* **2014**, *47*, 2582.
73 T. Wassmann, A. P. Seitsonen, A. M. Saitta, M. Lazzeri, F. Mauri, *J. Am. Chem. Soc.* **2010**, *132*, 3440.
74 T. Kubo, *Chem. Rec.* **2015**, *15*, 218.
75 A. Konishi, Y. Hirao, M. Nakano, A. Shimizu, E. Botek, B. Champagne, D. Shiomi, K. Sato, T. Takui, K. Matsumoto, H. Kurata, T. Kubo, *J. Am. Chem. Soc.* **2010**, *132*, 11021.
76 A. Konishi, Y. Hirao, K. Matsumoto, H. Kurata, R. Kishi, Y. Shigeta, M. Nakano, K. Tokunaga, K. Kamada, T. Kubo, *J. Am. Chem. Soc.* **2013**, *135*, 1430.
77 M. R. Ajayakumar, Y. B. Fu, J. Ma, F. Hennersdorf, H. Komber, J. J. Weigand, A. Alfonsov, A. A. Popov, R. Berger, J. Z. Liu, K. Müllen, X. L. Feng, *J. Am. Chem. Soc.* **2018**, *140*, 6240.
78 Y. Ni, T. Y. Gopalakrishna, H. Phan, T. S. Herng, S. F. Wu, Y. Han, J. Ding, J. S. Wu, *Angew. Chem., Int. Ed.* **2018**, *57*, 9697.
79 Y. W. Gu, X. J. Wu, T. Y. Gopalakrishna, H. Phan, J. S. Wu, *Angew. Chem., Int. Ed.* **2018**, *57*, 6541.
80 V. Bonal, R. Munoz-Marmol, F. Gordillo Gamez, M. Morales-Vidal, J. M. Villalvilla, P. G. Boj, J. A. Quintana, Y. Gu, J. Wu, J. Casado, M. A. Diaz-Garcia, *Nat. Commun.* **2019**, *10*, 3327.
81 T. Dumslaff, B. Yang, A. Maghsoumi, G. Velpula, K. S. Mali, C. Castiglioni, S. De Feyter, M. Tommasini, A. Narita, X. Feng, K. Müllen, *J. Am. Chem. Soc.* **2016**, *138*, 4726.
82 T. L. Yao, M. A. Campo, R. C. Larock, *J. Org. Chem.* **2005**, *70*, 3511.
83 G. M. Paternò, Q. Chen, X.-Y. Wang, J. Liu, S. G. Motti, A. Petrozza, X. Feng, G. Lanzani, K. Müllen, A. Narita, F. Scotognella, *Angew. Chem., Int. Ed.* **2017**, *56*, 6753.
84 T.-A. Chen, R.-S. Liu, *Chem.—Eur. J.* **2011**, *17*, 8023.
85 D. M. Coles, Q. Chen, L. C. Flatten, J. M. Smith, K. Müllen, A. Narita, D. G. Lidzey, *Nano Lett.* **2017**, *17*, 5521.
86 R. K. Mohamed, S. Mondal, J. V. Guerrera, T. M. Eaton, T. E. Albrecht-Schmitt, M. Shatruk, I. V. Alabugin, *Angew. Chem., Int. Ed.* **2016**, *55*, 12054.
87 Q. Chen, S. Thoms, S. Stöttinger, D. Schollmeyer, K. Müllen, A. Narita, T. Basché, *J. Am. Chem. Soc.* **2019**, *141*, 16439.
88 Q. Chen, W. Zajaczkowski, J. Seibel, S. De Feyter, W. Pisula, K. Müllen, A. Narita, *J. Mater. Chem. C* **2019**, *7*, 12898.
89 G. M. Paternò, L. Moretti, A. J. Barker, Q. Chen, K. Müllen, A. Narita, G. Cerullo, F. Scotognella, G. Lanzani, *Adv. Funct. Mater.* **2019**, *29*, 1805249.
90 G. M. Paternò, L. Nicoli, Q. Chen, K. Müllen, A. Narita, G. Lanzani, F. Scotognella, *J. Phys. Chem. C* **2018**, *122*, 25007.
91 Q. Chen, D. Schollmeyer, K. Müllen, A. Narita, *J. Am. Chem. Soc.* **2019**, doi:10.1021/jacs.9b10957.
92 X. M. Liu, S. Y. Chen, Q. Chen, X. L. Yao, M. Gelleri, S. Ritz, S. Kumar, C. Cremer, K. Landfester, K. Müllen, S. H. Parekh, A. Narita, M. Bonn, *Angew. Chem., Int. Ed.*, doi:10.1002/anie.201909220.
93 Q. Chen, D. Wang, M. Baumgarten, D. Schollmeyer, K. Müllen, A. Narita, *Chem.—Asian J.* **2019**, *14*, 1703.
94 R. D. Broene, F. Diederich, *Tetrahedron Lett.* **1991**, *32*, 5227.
95 C. Rogers, C. Chen, Z. Pedramrazi, A. A. Omrani, H.-Z. Tsai, H. S. Jung, S. Lin, M. F. Crommie, F. R. Fischer, *Angew. Chem., Int. Ed.* **2015**, *54*, 15143.
96 X.-Y. Wang, X. Yao, A. Narita, K. Müllen, *Acc. Chem. Res.* **2019**, *52*, 2491.
97 X. Y. Wang, F. Zhang, K. S. Schellharnmer, P. Machata, F. Ortmann, G. Cuniberti, Y. B. Fu, J. Hunger, R. Z. Tang, A. A. Popov, R. Berger, K. Müllen, X. L. Feng, *J. Am. Chem. Soc.* **2016**, *138*, 11606.
98 X.-Y. Wang, A. Narita, W. Zhang, X. Feng, K. Müllen, *J. Am. Chem. Soc.* **2016**, *138*, 9021.
99 T. Hatakeyama, S. Hashimoto, S. Seki, M. Nakamura, *J. Am. Chem. Soc.* **2011**, *133*, 18614.
100 X.-Y. Wang, T. Dienel, M. Di Giovannantonio, G. B. Barin, N. Kharche, O. Deniz, J. I. Urgel, R. Widmer, S. Stolz, L. H. De Lima, M. Muntwiler, M. Tommasini, V. Meunier, P. Ruffieux, X. Feng, R. Fasel, K. Müllen, A. Narita, *J. Am. Chem. Soc.* **2017**, *139*, 4671.
101 L. Chen, L. Wang, D. Beljonne, *Carbon* **2014**, *77*, 868.
102 B. Purushothaman, M. Bruzek, S. R. Parkin, A. F. Miller, J. E. Anthony, *Angew. Chem., Int. Ed.* **2011**, *50*, 7013.
103 R. Dorel, A. M. Echavarren, *Eur. J. Org. Chem.* **2017**, 14.
104 Y. Hu, X.-Y. Wang, P.-X. Peng, X.-C. Wang, X.-Y. Cao, X. Feng, K. Müllen, A. Narita, *Angew. Chem., Int. Ed.* **2017**, *56*, 3374.
105 Q. Zhong, Y. Hu, K. Niu, H. Zhang, B. Yang, D. Ebeling, J.

Tschakert, T. Cheng, A. Schirmeisen, A. Narita, K. Müllen, L. Chi, *J. Am. Chem. Soc.* **2019**, *141*, 7399.
106 K. Dhbaibi, L. Favereau, J. Crassous, *Chem. Rev.* **2019**, *119*, 8846.
107 M. Gingras, G. Felix, R. Peresutti, *Chem. Soc. Rev.* **2013**, *42*, 1007.
108 M. Gingras, *Chem. Soc. Rev.* **2013**, *42*, 1051.
109 M. Hasan, V. Borovkov, *Symmetry* **2018**, *10*, 10.
110 J. R. Brandt, F. Salerno, M. J. Fuchter, *Nat. Rev. Chem.* **2017**, *1*, 0045.
111 K. Mori, T. Murase, M. Fujita, *Angew. Chem., Int. Ed.* **2015**, *54*, 6847.
112 E. Clar, C. T. Ironside, M. Zander, *J. Chem. Soc.* **1959**, 142.
113 H. Kashihara, T. Asada, K. Kamikawa, *Chem.—Eur. J.* **2015**, *21*, 6523.
114 Y. Segawa, T. Maekawa, K. Itami, *Angew. Chem., Int. Ed.* **2015**, *54*, 66.
115 T. Katayama, S. Nakatsuka, H. Hirai, N. Yasuda, J. Kumar, T. Kawai, T. Hatakeyama, *J. Am. Chem. Soc.* **2016**, *138*, 5210.
116 X.-Y. Wang, X.-C. Wang, A. Narita, M. Wagner, X.-Y. Cao, X. Feng, K. Müllen, *J. Am. Chem. Soc.* **2016**, *138*, 12783.
117 Y. Hu, G. M. Paternò, X.-Y. Wang, X.-C. Wang, M. Guizzardi, Q. Chen, D. Schollmeyer, X.-Y. Cao, G. Cerullo, F. Scotognella, K. Müllen, A. Narita, *J. Am. Chem. Soc.* **2019**, *141*, 12797.
118 R. S. Jordan, Y. Wang, R. D. McCurdy, M. T. Yeung, K. L. Marsh, S. I. Khan, R. B. Kaner, Y. Rubin, *Chem* **2016**, *1*, 78.
119 R. S. Jordan, Y. L. Li, C.-W. Lin, R. D. McCurdy, J. B. Lin, J. L. Brosmer, K. L. Marsh, S. I. Khan, K. N. Houk, R. B. Kaner, Y. Rubin, *J. Am. Chem. Soc.* **2017**, *139*, 15878.
120 Y. Yano, N. Mitoma, K. Matsushima, F. Wang, K. Matsui, A. Takakura, Y. Miyauchi, H. Ito, K. Itami, *Nature* **2019**, *571*, 387.
121 Y.-C. Chen, D. G. de Oteyza, Z. Pedramrazi, C. Chen, F. R. Fischer, M. F. Crommie, *ACS Nano* **2013**, *7*, 6123.
122 A. Kimouche, M. M. Ervasti, R. Drost, S. Halonen, A. Harju, P. M. Joensuu, J. Sainio, P. Liljeroth, *Nat. Commun.* **2015**, *6*, 10177.
123 M. Mehdi Pour, A. Lashkov, A. Radocea, X. Liu, T. Sun, A. Lipatov, R. A. Korlacki, M. Shekhirev, N. R. Aluru, J. W. Lyding, V. Sysoev, A. Sinitskii, *Nat. Commun.* **2017**, *8*, 820.
124 T. H. Vo, M. Shekhirev, A. Lipatov, R. A. Korlacki, A. Sinitskii, *Faraday Discuss.* **2014**, *173*, 105.
125 R. A. Durr, D. Haberer, Y. L. Lee, R. Blackwell, A. M. Kalayjian, T. Marangoni, J. Ihm, S. G. Louie, F. R. Fischer, *J. Am. Chem. Soc.* **2018**, *140*, 807.
126 J. Liu, B.-W. Li, Y.-Z. Tan, A. Giannakopoulos, C. Sanchez-Sanchez, D. Beljonne, P. Ruffieux, R. Fasel, X. Feng, K. Müllen, *J. Am. Chem. Soc.* **2015**, *137*, 6097.
127 N. Mitoma, Y. Yano, H. Ito, Y. Miyauchi, K. Itami, *ACS Appl. Nano Mater.* **2019**, *2*, 4825.
128 D. G. de Oteyza, A. Garcia-Lekue, M. Vilas-Varela, N. Merino-Diez, E. Carbonell-Sanroma, M. Corso, G. Vasseur, C. Rogero, E. Guitian, J. I. Pascual, J. E. Ortega, Y. Wakayama, D. Pena, *ACS Nano* **2016**, *10*, 9000.
129 S. Kawai, S. Saito, S. Osumi, S. Yamaguchi, A. S. Foster, P. Spijker, E. Meyer, *Nat. Commun.* **2015**, *6*, 8098.
130 R. R. Cloke, T. Marangoni, G. D. Nguyen, T. Joshi, D. J. Rizzo, C. Bronner, T. Cao, S. G. Louie, M. F. Crommie, F. R. Fischer, *J. Am. Chem. Soc.* **2015**, *137*, 8872.
131 S. Kawai, S. Nakatsuka, T. Hatakeyama, R. Pawlak, T. Meier, J. Tracey, E. Meyer, A. S. Foster, *Sci. Adv.* **2018**, *4*, eaar7181.
132 J. Cai, C. A. Pignedoli, L. Talirz, P. Ruffieux, H. Söde, L. Liang, V. Meunier, R. Berger, R. Li, X. Feng, K. Müllen, R. Fasel, *Nat. Nanotechnol.* **2014**, *9*, 896.
133 Y.-F. Zhang, Y. Zhang, G. Li, J. Lu, Y. Que, H. Chen, R. Berger, X. Feng, K. Müllen, X. Lin, Y.-Y. Zhang, S. Du, S. T. Pantelides, H.-J. Gao, *Nano Res.* **2017**, *10*, 3377.
134 O. Deniz, C. Sánchez-Sánchez, T. Dumslaff, X. Feng, A. Narita, K. Müllen, N. Kharche, V. Meunier, R. Fasel, P. Ruffieux, *Nano Lett.* **2017**, *17*, 2197.
135 Y.-C. Chen, T. Cao, C. Chen, Z. Pedramrazi, D. Haberer, D. G. de Oteyza, F. R. Fischer, S. G. Louie, M. F. Crommie, *Nat. Nanotechnol.* **2015**, *10*, 156.
136 S. Y. Wang, N. Kharche, E. C. Girao, X. L. Feng, K. Müllen, V. Meunier, R. Fasel, P. Ruffieux, *Nano Lett.* **2017**, *17*, 4277.
137 X.-Y. Wang, J. I. Urgel, G. B. Barin, K. Eimre, M. Di Giovannantonio, A. Milani, M. Tommasini, C. A. Pignedoli, P. Ruffieux, X. Feng, R. Fasel, K. Müllen, A. Narita, *J. Am. Chem. Soc.* **2018**, *140*, 9104.
138 O. Gröning, S. Wang, X. Yao, C. A. Pignedoli, G. Borin Barin, C. Daniels, A. Cupo, V. Meunier, X. Feng, A. Narita, K. Müllen, P. Ruffieux, R. Fasel, *Nature* **2018**, *560*, 209.
139 S. Wang, L. Talirz, C. A. Pignedoli, X. Feng, K. Müllen, R. Fasel, P. Ruffieux, *Nat. Commun.* **2016**, *7*, 11507.
140 D. T. Chase, B. D. Rose, S. P. McClintock, L. N. Zakharov, M. M. Haley, *Angew. Chem., Int. Ed.* **2011**, *50*, 1127.
141 X. Y. Fu, D. H. Zhao, *Org. Lett.* **2015**, *17*, 5694.
142 A. Shimizu, R. Kishi, M. Nakano, D. Shiomi, K. Sato, T. Takui, I. Hisaki, M. Miyata, Y. Tobe, *Angew. Chem., Int. Ed.* **2013**, *52*, 6076.
143 C. K. Frederickson, B. D. Rose, M. M. Haley, *Acc. Chem. Res.* **2017**, *50*, 977.
144 M. Di Giovannantonio, J. I. Urgel, U. Beser, A. V. Yakutovich, J. Wilhelm, C. A. Pignedoli, P. Ruffieux, A. Narita, K. Müllen, R. Fasel, *J. Am. Chem. Soc.* **2018**, *140*, 3532.
145 M. Di Giovannantonio, K. Eimre, A. V. Yakutovich, Q. Chen, S. Mishra, J. I. Urgel, C. A. Pignedoli, P. Ruffieux, K. Müllen, A. Narita, R. Fasel, *J. Am. Chem. Soc.* **2019**, *141*, 12346.
146 J. M. Englert, J. Malig, V. A. Zamolo, A. Hirsch, N. Jux, *Chem. Commun.* **2013**, *49*, 4827.
147 S. Laschat, A. Baro, N. Steinke, F. Giesselmann, C. Hagele, G. Scalia, R. Judele, E. Kapatsina, S. Sauer, A. Schreivogel, M. Tosoni, *Angew. Chem., Int. Ed.* **2007**, *46*, 4832.
148 T. Wohrle, I. Wurzbach, J. Kirres, A. Kostidou, N. Kapernaum, J. Litterscheidt, J. C. Haenle, P. Staffeld, A. Baro, F. Giesselmann, S. Laschat, *Chem. Rev.* **2016**, *116*, 1139.
149 L. Chen, K. S. Mali, S. R. Puniredd, M. Baumgarten, K. Parvez, W. Pisula, S. De Feyter, K. Müllen, *J. Am. Chem. Soc.* **2013**, *135*, 13531.
150 R. Baumgartner, H. L. Fu, Z. Y. Song, Y. Lin, J. J. Cheng, *Nat. Chem.* **2017**, *9*, 614.
151 M. Hirai, N. Tanaka, M. Sakai, S. Yamaguchi, *Chem. Rev.* **2019**, *119*, 8291.
152 L. F. Dössel, V. Kamm, I. A. Howard, F. Laquai, W. Pisula, X. Feng, C. Li, M. Takase, T. Kudernac, S. De Feyter, K. Müllen, *J. Am. Chem. Soc.* **2012**, *134*, 5876.
153 W. W. H. Wong, T. Khoury, D. Vak, C. Yan, D. J. Jones, M. J. Crossley, A. B. Holmes, *J. Mater. Chem.* **2010**, *20*, 7005.
154 Y. Hu, P. Xie, M. De Corato, A. Ruini, S. Zhao, F. Meggendorfer, L. A. Straasø, L. Rondin, P. Simon, J. Li, J. J. Finley, M. R. Hansen, J.-S. Lauret, E. Molinari, X. Feng, J. V. Barth, C.-A. Palma, D. Prezzi, K. Müllen, A. Narita, *J. Am. Chem.*

Soc. **2018**, *140*, 7803.
155 A. Narita, I. A. Verzhbitskiy, W. Frederickx, K. S. Mali, S. A. Jensen, M. R. Hansen, M. Bonn, S. De Feyter, C. Casiraghi, X. Feng, K. Müllen, *ACS Nano* **2014**, *8*, 11622.
156 A. Keerthi, B. Radha, D. Rizzo, H. Lu, V. Diez Cabanes, I. C.-Y. Hou, D. Beljonne, J. Cornil, C. Casiraghi, M. Baumgarten, K. Müllen, A. Narita, *J. Am. Chem. Soc.* **2017**, *139*, 16454.
157 A. Keerthi, I. C.-Y. Hou, T. Marszalek, W. Pisula, M. Baumgarten, A. Narita, *Chem.—Asian J.* **2016**, *11*, 2710.
158 M. Slota, A. Keerthi, W. K. Myers, E. Tretyakov, M. Baumgarten, A. Ardavan, H. Sadeghi, C. J. Lambert, A. Narita, K. Müllen, L. Bogani, *Nature* **2018**, *557*, 691.
159 R. Tanimoto, S. Suzuki, M. Kozaki, K. Okada, *Chem. Lett.* **2014**, *43*, 678.
160 H. Sakaguchi, Y. Kawagoe, Y. Hirano, T. Iruka, M. Yano, T. Nakae, *Adv. Mater.* **2014**, *26*, 4134.
161 H. Sakaguchi, S. Song, T. Kojima, T. Nakae, *Nat. Chem.* **2017**, *9*, 57.
162 Z. Chen, W. Zhang, C.-A. Palma, A. Lodi Rizzini, B. Liu, A. Abbas, N. Richter, L. Martini, X.-Y. Wang, N. Cavani, H. Lu, N. Mishra, C. Coletti, R. Berger, F. Klappenberger, M. Kläui, A. Candini, M. Affronte, C. Zhou, V. De Renzi, U. del Pennino, J. V. Barth, H. J. Räder, A. Narita, X. Feng, K. Müllen, *J. Am. Chem. Soc.* **2016**, *138*, 15488.
163 Z. Chen, H. I. Wang, J. Teyssandier, K. S. Mali, T. Dumslaff, I. Ivanov, W. Zhang, P. Ruffieux, R. Fasel, H. J. Räder, D. Turchinovich, S. De Feyter, X. Feng, M. Kläui, A. Narita, M. Bonn, K. Müllen, *J. Am. Chem. Soc.* **2017**, *139*, 3635.
164 P. B. Bennett, Z. Pedramrazi, A. Madani, Y.-C. Chen, D. G. de Oteyza, C. Chen, F. R. Fischer, M. F. Crommie, J. Bokor, *Appl. Phys. Lett.* **2013**, *103*, 253114.
165 Z. Chen, H. I. Wang, N. Bilbao, J. Teyssandier, T. Prechtl, N. Cavani, A. Tries, R. Biagi, V. De Renzi, X. Feng, M. Kläui, S. De Feyter, M. Bonn, A. Narita, K. Müllen, *J. Am. Chem. Soc.* **2017**, *139*, 9483.
166 R. Saito, M. Furukawa, G. Dresselhaus, M. S. Dresselhaus, *J. Phys.: Condens. Matter* **2010**, *22*, 334203.
167 D. Prezzi, D. Varsano, A. Ruini, A. Marini, E. Molinari, *Phys. Rev. B: Condens. Matter Mater. Phys.* **2008**, *77*, 041404.
168 Z. Chen, R. Berger, K. Müllen, A. Narita, *Chem. Lett.* **2017**, *46*, 1476.